water

MDPI

Article

Spatial Distribution of Trace Elements in Sub-Surficial Marine Sediments: New Insights from Bay I of the Mar Piccolo of Taranto (Southern Italy)

Antonella Marsico [1,2], Angela Rizzo [1,2,*], Domenico Capolongo [1,2], Francesco De Giosa [3], Antonella Di Leo [4], Stefania Lisco [1,2], Giuseppe Mastronuzzi [1,2], Massimo Moretti [1,2], Giovanni Scardino [1,2] and Giovanni Scicchitano [1,2]

[1] Department of Earth and Geoenvironmental Sciences, University of Bari Aldo Moro, Campus Universitario, Via E. Orabona, 4, 70125 Bari, Italy
[2] Interdepartmental Research Centre for Coastal Dynamics, University of Bari Aldo Moro, Via E. Orabona, 4, 70125 Bari, Italy
[3] Environmental Surveys S.r.l., Via Renato Dario Lupo, 65, 74121 Taranto, Italy
[4] Istituto di Ricerca sulle Acque (IRSA) Consiglio Nazionale delle Ricerche, Via Roma, 3, 74123 Taranto, Italy
* Correspondence: angela.rizzo@uniba.it

Abstract: Contaminated marine and coastal sediments represent the main source of secondary pollution for the aquatic environment and marine fauna, affecting, directly and indirectly, ecosystems and human health. The assessment of the distribution of chemical pollutants in marine sediments can therefore be considered a preliminary step for understanding the possible circulation of pollutants in the marine environment and planning any targeted and efficient reclamation activity. This study provides new insights on the environmental status of Bay I of Mar Piccolo basin (Southern Italy) by proposing an integrated investigation approach to define the distribution of trace metals and evaluate the thickness of the sediments potentially affected by pollution. To this aim, the concentrations of As, Cd, Cr, Cu, Hg, Ni, Pb, Sn, and Zn are estimated for sediment samples collected from 19 cores, and specific environmental indices are calculated. Due to its remarkable environmental and economic relevance, the area of Taranto has been selected as a case study to evaluate the effectiveness of the proposed method in supporting the identification of hotspot areas for which priority remediation activities are needed.

Keywords: geo-environmental surveys; marine sediment pollution; coastal geomorphology; trace metals; risk maps; pollution indices

Citation: Marsico, A.; Rizzo, A.; Capolongo, D.; De Giosa, F.; Di Leo, A.; Lisco, S.; Mastronuzzi, G.; Moretti, M.; Scardino, G.; Scicchitano, G. Spatial Distribution of Trace Elements in Sub-Surficial Marine Sediments: New Insights from Bay I of the Mar Piccolo of Taranto (Southern Italy). *Water* **2023**, *15*, 3642. https://doi.org/10.3390/w15203642

Academic Editor: Bahram Gharabaghi

Received: 5 September 2023
Revised: 2 October 2023
Accepted: 12 October 2023
Published: 17 October 2023

1. Introduction

Marine and coastal sediments are often used as an indicator for the evaluation of the environmental status of aquatic environments because they act as storage tanks for pollutants [1,2]. Sediments are therefore considered the most conservative environmental matrix and represent the final sink of most anthropogenic contaminants, thus playing a primary role both in the accumulation of pollutants through the deposition of suspended particles and adsorption by clay minerals and in their redistribution [3]. Inorganic compounds and trace elements, whose presence in coastal zones can be attributed to both natural processes and anthropogenic activities [4] and reference therein, are characterized by high persistence in the various environmental matrices and can lead to bioaccumulation with consequent negative impacts on ecosystems. The presence of high concentrations of trace metals in the marine sediments represents a global issue since worldwide the coastal areas host the highest density of anthropogenic activities, including industrial systems [metallurgical, steel, chemical, pharmaceutical, petrochemical, mechanical], arsenals, landfills, shipyards, and harbors, with the related high maritime bustle [5–10].

Due to their specific morphodynamic characteristics, enclosed coastal systems (e.g., areas where wide sand spit forms natural barriers) may be characterized by greater accumulation of pollutants due to the limited water circulation, resulting in low self-purification capacity of the system [11,12].

A high number of contaminated sites are located along the Italian coastal sector, and, among these, 17 are included in the list of sites of national interest (SINs), which represent territories entailing high health and ecological risk whose management is directly entrusted to the Environmental Ministry (now the Ministry of Environment and Energy Security, MASE). Ausili et al. [3,13] have proposed a common investigation strategy for the analysis of the contaminants' distribution in marine areas by considering all the environmental matrices (water, sediments, and biota). The contamination level of several Italian SINs has been the subject of study in the frame of scientific and technical projects. One of the most investigated high-contaminated areas is Augusta Bay (Sicily, Southern Italy), which hosts the "SIN_04 Priolo" [14–18]. A high number of scientific studies have been focused on the characterization of the "SIN_17 Bagnoli", whose contamination is mainly due to a steel/metallurgic plant in function from 1910 to 1992 [19–23].

In this study, new insights on the environmental conditions of the coastal areas included in "SIN_07—Taranto" are provided by analyzing the spatial distribution of trace metals in the superficial and sub-surficial sediments of the Mar Piccolo basin, a semi-enclosed basin in the Apulia Region (Southern Italy), included in the SIN perimeter. Due to its remarkable environmental and ecological importance, the area has been subject to intensive characterization activities during the last decades carried out by national and regional agencies (ICRAM and ARPA, respectively). Furthermore, the chemical characterization of the marine sediments of the Mar Piccolo has been previously analyzed by several authors [24]. The results of such characterizations highlighted that in general (i) seawater and sediment showed a high level of contamination, (ii) Hg was the most widespread contaminant, and (iii) the consistency of shallow sediments ranges from largely fluid to soft [25,26].

More recently, the area has been further investigated during the characterization surveys funded by the "Special Commissioner for urgent measures of reclamation, environmental improvements, and redevelopment of Taranto", during which a multidisciplinary approach has been applied to enhance the conceptual site model [27]. With the main aim of analyzing the 3D distribution of the trace metal in the uppermost 3 m of sediments, 19 cores have been analyzed here by applying specific interpolation tools and geo-environmental indices. Furthermore, by interpreting high-resolution seismic data (sub-bottom profiler data), the vertical distribution of different sediment units has been assessed.

The analyses proposed in the study are aimed at providing a methodological approach for supporting the characterization of highly polluted coastal sites by promoting the integrated exploitation of data acquired following national procedures. The analysis steps include the evaluation of the As, Cd, Cr, Cu, Hg, Ni, Pb, Sn, and Zn concentrations and the calculation of specific indices, which allow the definition of the environmental status of the marine sediments. Then, by interpreting seismic signals, the thickness of the most surficial sub-surficial marine sediment layers is estimated. The results, which are proposed in the form of tables and maps, allow the identification of "hot-spot areas", that is, areas in which the concentrations of more than one contaminant are above the limit values. Such information, in association with the data obtained as part of the multidisciplinary study to improve the conceptual model of the site, can be considered the preparatory layers to define risk scenarios and address tailored remediation activities.

2. Study Area

The Taranto area (Figure 1) is located on the northern Ionian coast in the southwestern Apulia region, between the eastern sector of the Bradanic Trough and the southwestern sector of the Apulian Foreland [28]. The Taranto landscape is characterized by a sequence of near-flat surfaces consisting of marine terrace deposits crossed by a fluvial network, which

is marked by a rectangular pattern and by two sub-circular basins, called Mar Grande and Mar Piccolo, literally "Big Sea" and "Little Sea" [29]. The semi-enclosed basin of Mar Piccolo is split into two connected sheltered bays by the Punta Penne promontory: The First (I) Bay and the Second (II) Bay, which are characterized by a mean water depth of 12 m and 8 m, respectively. The Mar Piccolo is connected to the Mar Grande by two channels: the shallow natural "Porta Napoli" channel and the artificial "Navigabile" channel, excavated during the XIX century [27]. The geology of the Taranto area is well known, and it is illustrated in the geological map published by Lisco et al. [30]. From the stratigraphical point of view, Upper Cretaceus limestone (Calcare di Altamura Formation) and Upper Pliocene–Lower Pleistocene calcarenite (Calcarenite di Gravina Formation) crop out in the northern sector of the Taranto area. Calcarenite di Gravina Fm. passes upward and toward S to the argille subappennine informal unit [28]. The geological framework is supplemented by: Middle–Upper Pleistocene marine, transitional and terraced deposits, and Holocene fluvial and marine deposits. In addition, a more recent study based on morpho-sedimentary data shows the evolution model of the Mar Piccolo basin [31]. In this study, the authors interpreted the evolution of Mar Piccolo as a result of the action of erosive and depositional processes that have developed in transitional low-energy environments combined with an incised-valley system during the last sea-level cycle. The same model attributes the high erodibility of the cliffs, combined with the interaction of the river incision, to the characteristic eight-shape of the current semi-closed basin of the Mar Piccolo.

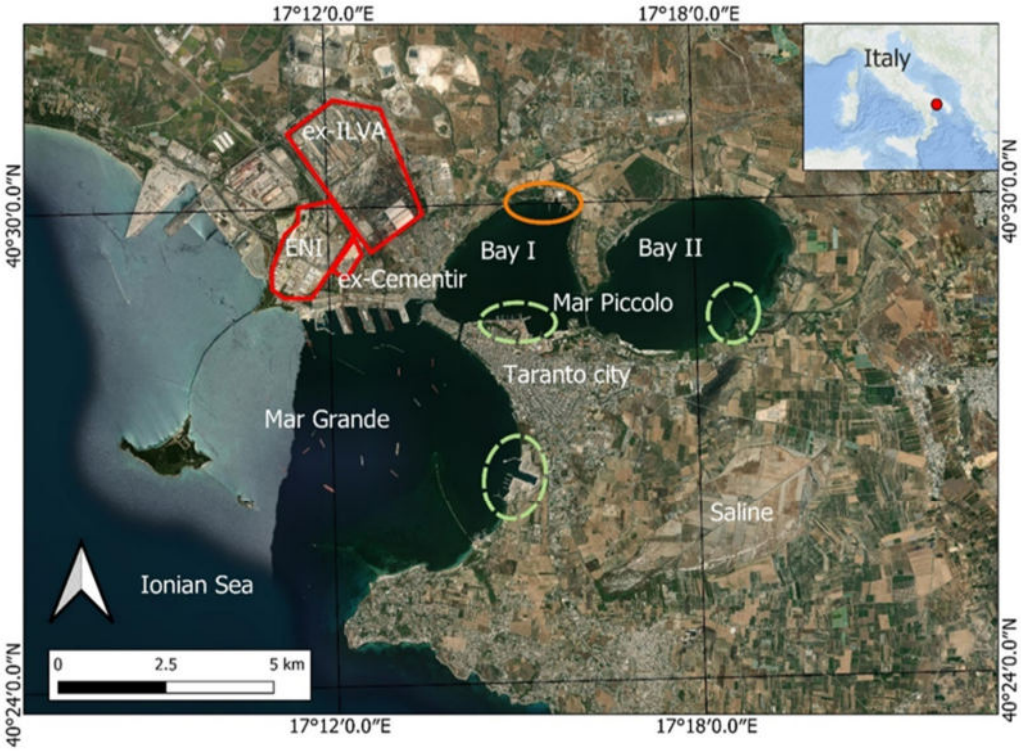

Figure 1. Study area location. The industrial sites are shown in red. The shipyards and dockyards of the Italian Navy (MG and MP—Bay I) and of the Italian Air Force (MP—Bay II) are identified by the green dashed circles. Finally, the orange circle identifies the ex-Tosi shipyard area.

From the analysis of the most recent literature data [31,32], it emerged that Bay I of the Mar Piccolo basin is characterized by quite high sediment accumulation rates, with values ranging from 1 mm/year to 3 mm/yr. With regards to the granulometric composition, results obtained by Dominik et al. [32] highlight that sediments from the I Bay are mainly clayey silt, with the silt fraction accounting for 60%, followed by clay (30%) and sand (10%). Furthermore, as emerged from the sediment core described in Valenzano et al. [31], the upper part of the sediment layer in the Mar Piccolo basin corresponds to specific lithofa-

cies, consisting of very soft, grey, structureless silts with an abundant organic content and bioclasts whose deposition occurred in a semi-enclosed basin with low hydro-dynamicity. The geomorphological setting provides to the Mar Piccolo basin a particular seawater circulation trigged by the submarine and subaerial freshwater springs representing the near-surface circulation engine toward the inlets and by the bottom currents moving in the system through the two inlets, Navigabile and Porta Napoli channels [33,34]. Peculiar transitional and shallow-marine habitats occur as a result of both the sea-water circulation and the massive presence of freshwater springs linked to a confined karst aquifer. Conversely to its high ecological importance, since the second half of the XIX century, the area has suffered intense environmental changes related to strong industrialization. The high-density urban centers, the presence of military harbor activities, steel, oil, and cement industries, and aquaculture plants have affected the health of the marine ecosystem, and the ecological balances have been strongly modified by the anthropogenic pressure connected to different sources of pollution [27,35–37]. Although land-based activities can be considered the main metal sources, runoff and surface transport processes, as well as atmospheric deposition, cannot be ruled out. As highlighted by previous characterization activities [27,38], the southernmost sector of Bay I, which is known as "Area 170 ha", is considered the most compromised marine sector.

Despite the heavy anthropogenic pressures, this area boasts an impressive naturalistic richness; hundreds of different species have been recorded in this basin [39,40]. In particular, recently, the widespread presence of the mollusc *Pinna nobilis* and some species of seahorses [41] has made the area a real biodiversity hot spot; indeed, much of the basin represents an area of habitat of naturalistic interest and is partially subject to protection.

3. Materials and Methods

With the main aim of evaluating the current environmental condition of Bay I of the Mar Piccolo basin, in this study, the 3D distribution of trace metals in the surficial and sub-surfial marine sediments is analyzed, and the thickness of the potentially contaminated layers is delineated. These evaluations are based on the integrated analysis of chemical (trace metals—TMs) and geophysical (sub-bottom profiler—SBP) data. The applied investigation approach is synthesized in the flowchart in Figure 2.

3.1. Data Acquisition

Acquisition and data analysis activities were financed by the "Special Commissioner for urgent measures of reclamation, environmental improvements, and redevelopment of Taranto" and were carried out through the Collaboration Agreement "Activities of common interest preparatory to the implementation of the interventions for the reclamation, environmentalization and requalification of the Mar Piccolo of Taranto". In detail, 19 survey cores were sampled in Bay I of the Mar Piccolo (Figure 3) during 2016 and 2017. Coring was carried out using a rotary corer mounted on board a barge with liners of 150 cm, from the seabed up to the lithostratigraphic contact with the underlying argille subappennine, at approximately 40 m. Each liner was properly sectioned to carry out sedimentological, geotechnical, and chemical analyses [27,42]. For the chemical analysis, each sample was divided into three sub-samples of 0.5 m. Sediment samples referred to ≈0–0.50 m, ≈0.50–1 m, and the ≈1.5–3 m layers were analyzed in detail in this study. Sub-bottom profiler (SBP) data were acquired by means of an INNOMAR SES-2000 compact multiparametric SBP, a seismic system with a primary frequency of 85–115 kHz. The SBP system was mounted on board R/V Issel, owned by *Consorzio Nazionale Interuniversitario per le Scienze del Mare* (CoNISMa). The navigation lines for the marine geophysical survey are shown in Figure 3. The preliminary analysis of the geophysical data allowed the recognition of the different seismic units.

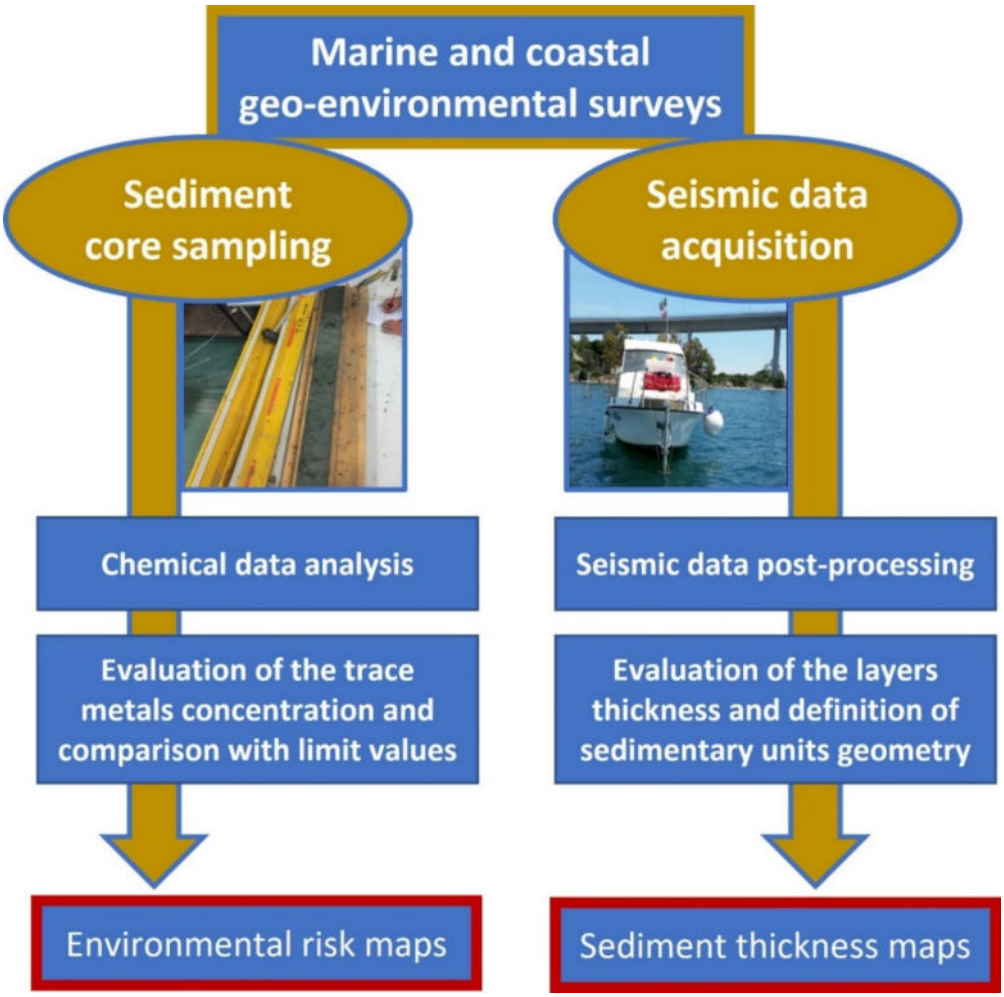

Figure 2. Schematic representation of the different analyses carried out to perform an integrated marine sediment characterization and to evaluate potential environmental risk scenarios.

3.2. Data Processing

To calculate the trace metal concentrations, the ICP–MS technique (EPA Method 6020B) was applied after acid digestion (HF + HNO_3) of sediments in a microwave oven (EPA Method 3052). For calibration, all standards were prepared in the same matrix as the one used for sediment analyses. Working standard solutions of metals were prepared with serial dilution of stock standard solutions of ultrapure grade supplied by Merck. To check for contamination, procedural blanks were analyzed in every five samples. Each sample was analyzed for three replicates (RSD 5–10%). The accuracy and precision of the analytical procedures were verified using the certified reference marine sediment, IAEA-356. The recovery percentage for certified reference marine sediment was in the range of 93% (Pb208) and 107% (Zn66). In detail, the first liner was split into three sub-samples of 0.5 m, while the second liner was analyzed in its entirety. Each sub-sample was mixed to form a representative composite sample of the analyzed depths (≈0–0.50 m, ≈0.50–1 m, and ≈1.5–3 m). Then, each sub-sample was subjected to chemical analysis. Nevertheless, the sub-sample relative to the depth of 1–1.50 m was not taken into consideration in this study since it was present only in a few cores.

In order to produce an overall environmental risk map for each of the analyzed depths, the following three-step procedure of analysis is proposed:

Step 1: The concentrations of As, Cd, Cr, Cu, Hg, Ni, Pb, Sn, and Zn estimated for each analyzed sub-sample were vectorized in the GIS environment and then interpolated by the

inverse distance weighting (IDW) method to assess and map their spatial distribution. The IDW method resulted in better preserving the values of the input dataset.

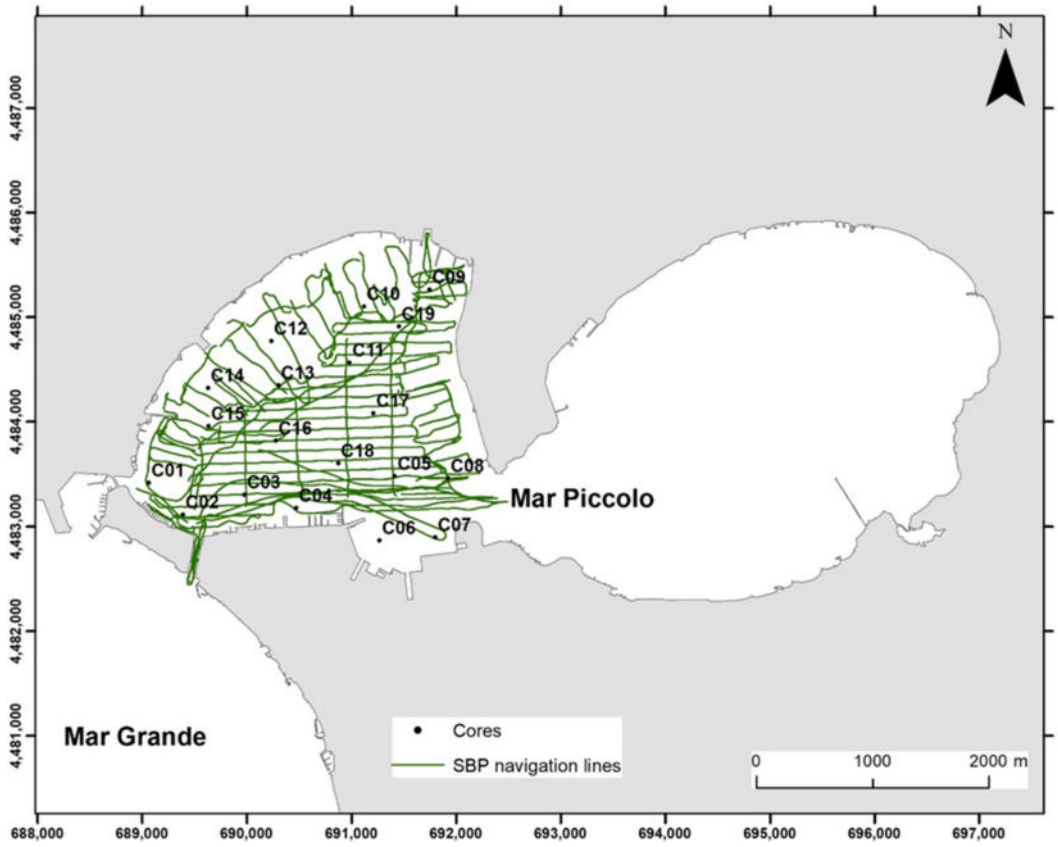

Figure 3. The black dots show the position of the sampling sites in Bay I of the Mar Piccolo basin while the green lines represent the traces followed for the sub-bottom profile (SBP) data acquisition.

Step 2: The concentration maps obtained in Step 1 for each contaminant at each analyzed depth were reclassified in four classes based on both the national limits (contamination threshold concentrations—CSC) identified for sites with both commercial and residential use (lower CSC values) and industrial use (higher CSC values) (cf. Annex 5 to Title V of Part IV of Legislative Decree no. 152/06 and ss.mm.ii.) and the site-specific action limits established for the SIN "Taranto" by ICRAM in 2004. Limit values are indicated in Table 1. Although CSC values refer to the soil, subsoil, and groundwater, they currently represent the reference values for the characterization and remediation activities of marine coastal areas.

Step 3: The reclassified concentration maps obtained in Step 2 were then overlapped and combined by a raster calculator analysis and then reclassified into four classes ranging from "low" to "very-high", in order to highlight the areas where one or more than one contaminant exceeded the limit values. In detail, the areas that fall in the low-risk level represent areas where the concentrations of all the accounted trace metals are under the above-mentioned limit values, whereas areas fall in the very-high class if at least one of the accounted trace metals is above the upper national limit values.

The thickness of sediment layers was evaluated by analyzing seismic data. To this aim, raw seismic data were converted into the SEGY format and processed by the IXSEA Delph software version 2020 (iXBlue, Denver, CO, USA). For each SBP seismic section, the reflectors corresponding to a change in the seismic impedance on the sediments were mapped. For the time/depth conversion, an average velocity of 1500 m/s for the water column and 1670 m/s for the sediments was used [27,31,42]. All acquired data were reported in a GIS environment. To obtain a digital model of the uppermost sediment layer

in Bay I of the Mar Piccolo basin, an interpolation process was performed through the natural-neighbor method.

Table 1. Site-specific limit values for the SIN "Taranto" and national limits (expressed in terms of CSC—cf. Legislative Decree 152/2006) are shown. Concentration limits are expressed in ppm (mg/kg dw) (a) refers to samples with a silt content < 20%, (b) refers to samples with a silt content > 20%, (*) identifies limits for sites with commercial and residential use, (**) identifies limits for sites with industrial use.

Limit Values	As	Cd	Cr	Cu	Hg	Ni	Pb	Sn	Zn
Taranto site-specific action levels	20	1	70 [a]/160 [b]	45	0.8	40 [a]/100 [b]	50	0.07	110
National limits (CSC *)	20	2	150	120	1	120	100	1	150
National limits (CSC **)	50	15	800	600	5	500	1000	350	1500

3.3. Pollution Analysis by Statistical Analysis, Indices, and Quality Standards

3.3.1. Statistical Analysis

Multivariate statistical analyses were carried out by the STATISTICA version 14 (StatSoft Inc., Tulsa, OK, USA) software package.

Principal component analysis (PCA) was performed on the data to provide a complete 3D distribution of the contaminants in the highly polluted marine basin. To recognize groups of samples with similar behavior and the correlation among the variables, a combined plot of scores and loadings was used.

The data set for the statistical analysis included 57 samples from the 19 sites, considering the three depth levels (0–0.50 m, 0.50–1 m, 1.5–3 m) and 9 variables, consisting of the values of concentration of As, Hg, Cr, Cu, Ni, Pb, Sn, Cd, and Zn.

3.3.2. Geoaccumulation Index, Enrichment Factor, Contamination Factor, Pollution Index, and Ecological Risk

The sources and extent of trace metal pollution in sediments were evaluated by calculating several pollution indicators, including the geoaccumulation index (Igeo), the enrichment factor (EF), the contamination factor (Cf), the modified contamination degree (mCd), and the pollution index (PLI).

In detail, the geoaccumulation index (Igeo), which helps to discover the degree of contamination [43], is:

$$\text{Igeo} = \log2\ (\text{Ci}/k\text{Bi}) \quad (1)$$

where Ci is the concentration of the examined heavy metal, Bi is the geochemical background value for the same metal, and k is the correction factor due to lithogenic effects (k = 1.5). Igeo values were classified following the ranges proposed by Muller [44], according to which values ranging from 4 to 5 identify strongly polluted sediments, while values higher than 5 identify very extremely polluted conditions.

The enrichment factor (EF) is a tool for estimating the degree of anthropogenic contamination by normalizing the measured heavy metal concentration (Ci) with respect to a reference metal such as Fe or Al [45], which act as clay content detectors [46,47]. EF was calculated using Fe as the reference element and according to the following formula [48]:

$$\text{EF} = \frac{\left(\frac{\text{Ci}}{\text{Fe}}\right)\text{Sample}}{\left(\frac{\text{Ci}}{\text{Fe}}\right)\text{Background}} \quad (2)$$

The contamination factor (Cf) of each metal was calculated to estimate the contamination of the single heavy metal in each sample [49,50]. The Cf is determined by the ratio

between the heavy metal concentration in the sediment and the concentration of the same metal in the background.

$$Cf = \frac{C(Sample)}{C(Background)} \quad (3)$$

The Cf values were classified according to the classification proposed by [51]. According to this classification, a Cf higher than 6 represents a very high contamination situation. From the Cf, two indices can be derived: the contamination degree (CD), which is the sum of the contamination factors, and the modified contamination degree (mCD), which allows to assess the contamination of all metals. The mCD index was calculated according to the following formula:

$$mCd = \frac{(\sum Cf)}{n} \quad (4)$$

According to the classification proposed by [52] and reported in Table 2, sediments with mCd values lower than 1.5 are characterized by a very low degree of contamination, while sediments with mCd values higher than 32 are characterized by an ultra-high degree of contamination.

Table 2. mCd classification and environmental interpretation according to [52].

mCd Range	Environmental Status
mCd < 1.5	Very low degree of contamination
1.5 ≤ mCd < 2	Low degree of contamination
2 ≤ mCd < 4	Moderate degree of contamination
4 ≤ mCd < 8	High degree of contamination
8 ≤ mCd < 16	Very high degree of contamination
16 ≤ mCd < 32	Extremely high degree of contamination
mCd ≥ 32	Ultra-high degree of contamination

The pollution index (PLI) combines any number of analyzed heavy metals computed according to the following formula [53]:

$$PLI = (Cf1 \times Cf2 \times Cf3 \times \ldots .Cfn)^{1/n} \quad (5)$$

where Cf is the contamination factor and "n" is the number of metals considered. As indicated in [53] and [54], sediments with a PLI value > 1 are considered polluted and therefore affected by anthropogenic inputs [55], while a PLI value < 1 indicates no contamination.

The potential ecological risk index (RI) that reflects the potential ecological impact of elements in sediment was calculated. This method comprehensively considers element toxicity [2], the sensitivity of the evaluation area to element pollution, and the difference in the background level of the metal area [56]. The ecological risk was calculated according to the following formulas [51,57]:

$$E_r = T_r \, X \, Cf \quad (6)$$

$$RI = \Sigma E_r \quad (7)$$

where Er is the potential ecological risk factor of a specific metal, Tr is the toxicity response factor of the metal, Cf is the contamination factor of metal, and RI (potential ecological risk index) is the sum of the potential risks of individual metals. The toxicity response factors of Zn, Cr, Cu, Ni, Pb, As, Cd, and Hg are 1, 2, 5, 5, 5, 10, 30, and 40, respectively, while the toxicity response factor for Sn is not available. Hakanson (1980) [51] defined 5 categories of Er and 4 categories of RI. So we have: for Er < 40, low ecological risk; for 40 < Er ≤ 80, moderate ecological risk; for 80 < Er ≤ 160, appreciable ecological risk; for 160 < Er ≤ 320, high ecological risk; and >320, serious ecological risk; for RI < 150, low ecological risk; for

150 < RI < 300, moderate ecological risk; for 300 < RI < 600, high ecological risk; and for RI $\geq$ 600, significantly high ecological risk.

The background values used for the calculation of Igeo, EF, and Cf refer to the values estimated in [24] for the Ionian area. Nevertheless, background values for As, Cd, and Sn refer to the average shale values [58].

3.3.3. Quality Standards

The Italian Law N. 172/2015 (Implementation of 2013/39/EU) establishes the Environmental Quality Standards (SQA in Italian), which represent a qualitative approach to assess if a particular pollutant or a group of pollutants in water, sediment, and biota poses issues for human health and the environment. Similarly, at the international level, a number of sediment quality guidelines based on tests have been proposed to predict the adverse biological effects caused by contaminated sediments. The lower tenth percentiles are defined as "effects range—low (ERL)" and the median as "effects range—median (ERM)". If the concentrations of contaminants trigger either of these values, further investigations are strongly required to assess environmental impacts. A comparison between the concentration of the trace metals and the international qualitative standard values shown in Table 3 is also presented.

Table 3. International sediment guideline limit values (ERL and ERM—[59]; TEL and PEL—[60]). Limits are expressed in ppm (mg/kg dw).

SQGs	As	Cd	Cr	Cu	Hg	Ni	Pb	Sn	Zn
ERL	8.2	1.2	81	34	0.15	20.9	46.7	-	150
ERM	70	9.6	370	270	0.71	51.6	218	-	410
TEL	7.24	0.68	52.3	18.7	0.13	15.9	30.2	-	124
PEL	41.6	4.21	160	108	0.7	42.8	112	-	271

4. Results

The distribution of the trace metals in the uppermost sedimentary layer (≈0–0.5 m, "Level_1" in Figures 4–6) shows that the most compromised areas in terms of metal contamination are located in the central-southern sector of Bay I. In particular, the Hg, As, and Zn concentrations follow the same trend, with the highest values in the southernmost cores of the basin, whereas the Ni and Cr content are highest in the central and northeastern parts of Bay I. Cd and Pb have the highest concentrations in the southern part of the area. Finally, the highest Cu and Sn concentrations are found in the central-western part.

The trace metal concentration in the second sediment layer (≈0.5–1 m, "Level_2" in Figures 4–6) shows a different pattern. The highest concentrations of Zn, Cd, and Cu are found in cores in the center of the bay, showing a different trend compared to the previous layer. The highest values of Pb have been detected in the southwestern and central cores; the concentrations of Hg and Sn show a homogeneous distribution, with a slightly high concentration of Sn in C16, whereas the highest concentration of As is in the center of Bay I. The highest values of Ni and Cr are found in the eastern part of Bay I, quite similar to the previous layer.

The spatial distribution of trace metals in the deepest analyzed layer (≈1.5–3 m, "Level_3" in Figures 4–6) is quite similar to the one in the second layer. In fact, Hg, Cd, and Pb present the same distribution pattern with their higher content in the southwestern part of the basin. Their highest value has been found in the core C03, in which also Zn reaches its highest concentration. As regards the distribution of Cu, it has the highest concentration in the central part of Bay I; in core C18, Cu reaches its highest value. In the same core, the concentration of Ni is lower. Instead, it shows the highest values in the central part of Bay I, similar to Cr concertation. The concentration of As is highest in the central and western

parts of the area, with values greater than those in Level_2, while the concentration of Sn is quite homogeneous at this depth.

Then, in order to evaluate the degree of contamination, the areal distribution of the investigated trace metals in the three layers is analyzed by comparing their concentrations with the site-specific limits established for the SIN of Taranto (ICRAM, 2004) and with the national CSC values (cf. Table 2). Results are reported in Table 4.

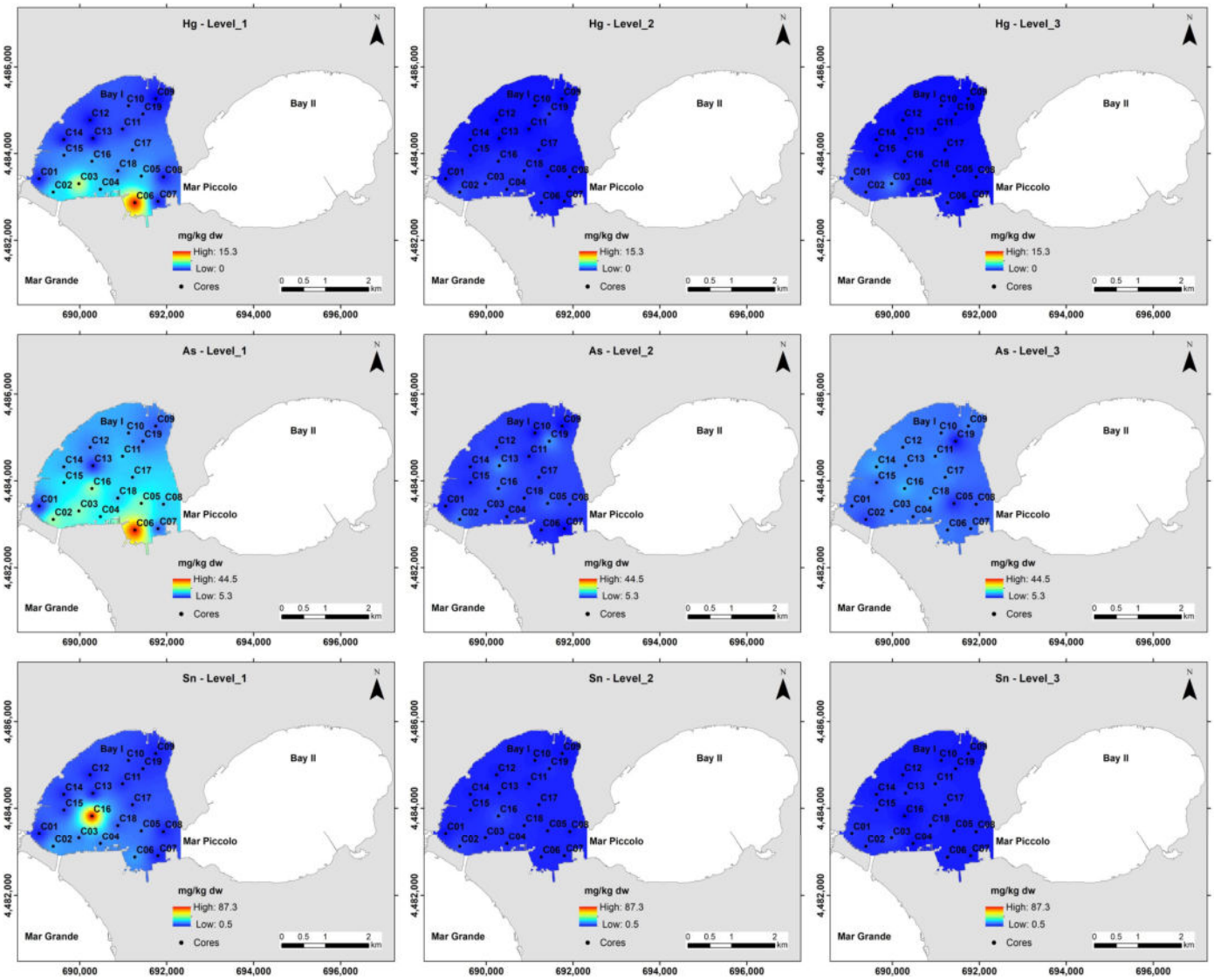

Figure 4. Spatial distribution of Hg, As, and Sn in the Mar Piccolo basin (Bay I): the concentration of each trace metal in the three analyzed levels (≈0–0.50 m, ≈0.50–1 m, and ≈1.5–3 m) is shown in the rows ("Level_01", "Level_2", and "Level_3", respectively).

In detail, the Hg content exceeds the highest CSC value only in Level_01 in cores C6 and C3 that are located in the "Area 170 ha". In cores C2, C4, C5, C16, C15, C18, C17, and C19, the Hg content exceeds the lower CSC value, too. In all the above-mentioned cores plus C11, the Hg concentrations at Level_01 exceed the limit value defined for the SIN of Taranto. In Level_02, Hg levels slightly exceed the site-specific limits in cores C2 and C3, and only in core C2 do they exceed the CSC lower value. Finally, at Level_03, both the values of the site-specific and the national limits (lower CSC) are exceeded in cores C3 and C1. Generally, the highest concentrations of Hg are found in the most superficial layers. Analyzing the vertical distribution of Hg in the three levels, it is possible to observe that in cores C1 and C10, the highest concentration of Hg was not found in the most superficial layer but in

Level_03 (≈1.5–3 m). This latter aspect could indicate that reworking phenomena may have occurred, as also highlighted in [61] for the organotin compounds.

The highest concentrations of Pb in Level_01, as for Hg, are found in cores located in the "Area 170 ha" (cores C3 and C6), while the lowest concentrations characterize the northeast and northwest parts of the basin. The distribution of Pb in the analyzed cores shows the same behavior as Hg since the highest concentrations are found in the same cores (cores C3 and C6). Nevertheless, differently from Hg, in no cores, the Pb concentration exceeds the national limit value (higher CSC), while the lower CSC value has always been exceeded in Level_01 (cores C2, C3, C6, C5, and C16). In addition, the site-specific limits are exceeded in cores C15, C17, and C18. Furthermore, the concentration of Pb in cores C16 and C18, located in the center of Bay I, exceeds the site-specific limit value even in Level_02. The highest concentrations of Pb are found in the most superficial layer and then settle on a constant value. Regarding the vertical distribution of Pb in the three analyzed levels, it is possible to observe that only in core C1, as for Hg, the highest concentration is not found in the most superficial layer but in Level_03, where the site-specific limit is also slightly exceeded. This could indicate that reworking phenomena may have occurred, as reported for Hg distribution.

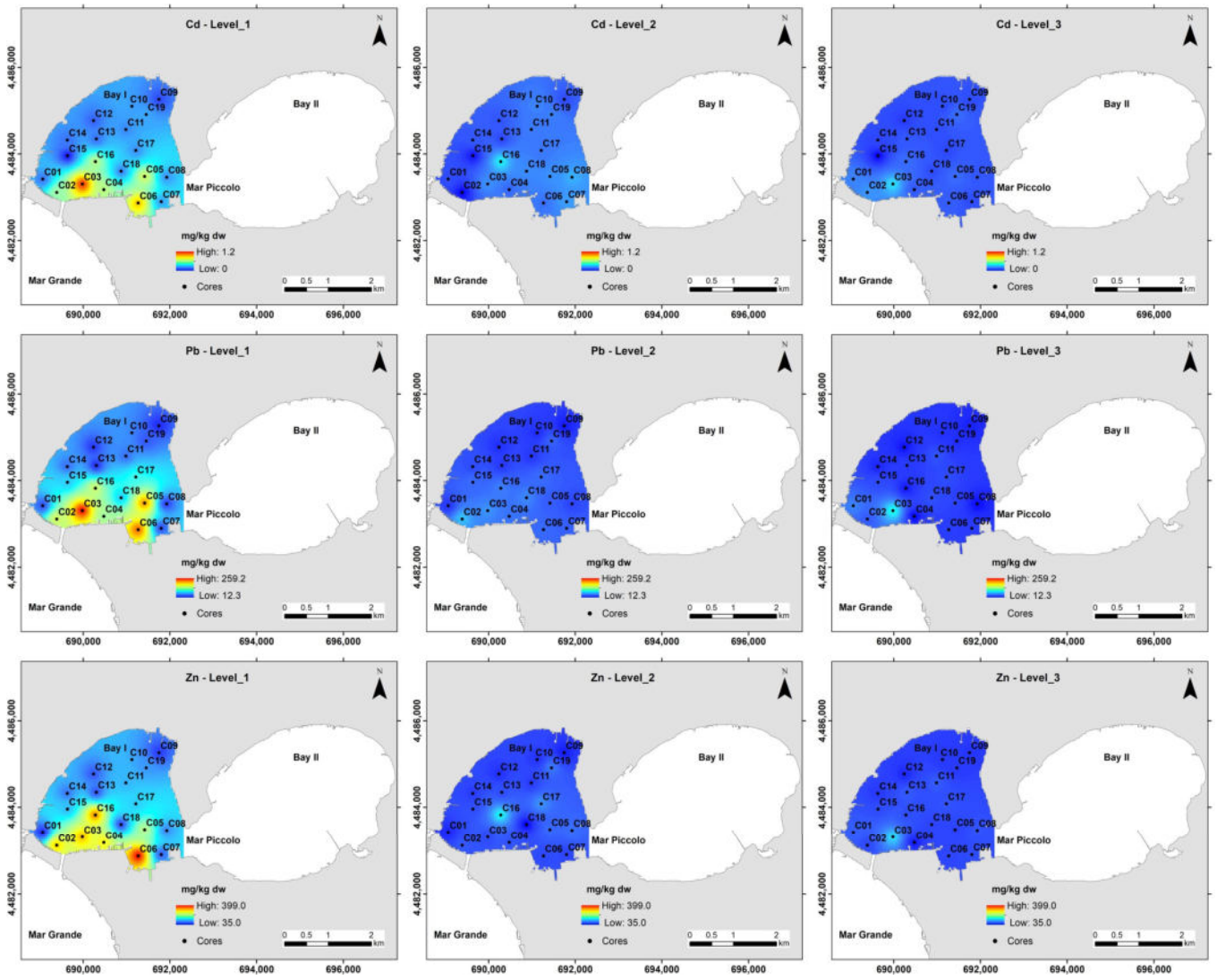

Figure 5. Spatial distribution of Cd, Pb, and Zn in the Mar Piccolo basin (Bay I): the concentration of each trace metal in the three analyzed levels (≈0–0.50 m, ≈0.50–1 m, and ≈1.5–3 m) is shown in the rows ("Level_01", "Level_2", and "Level_3", respectively).

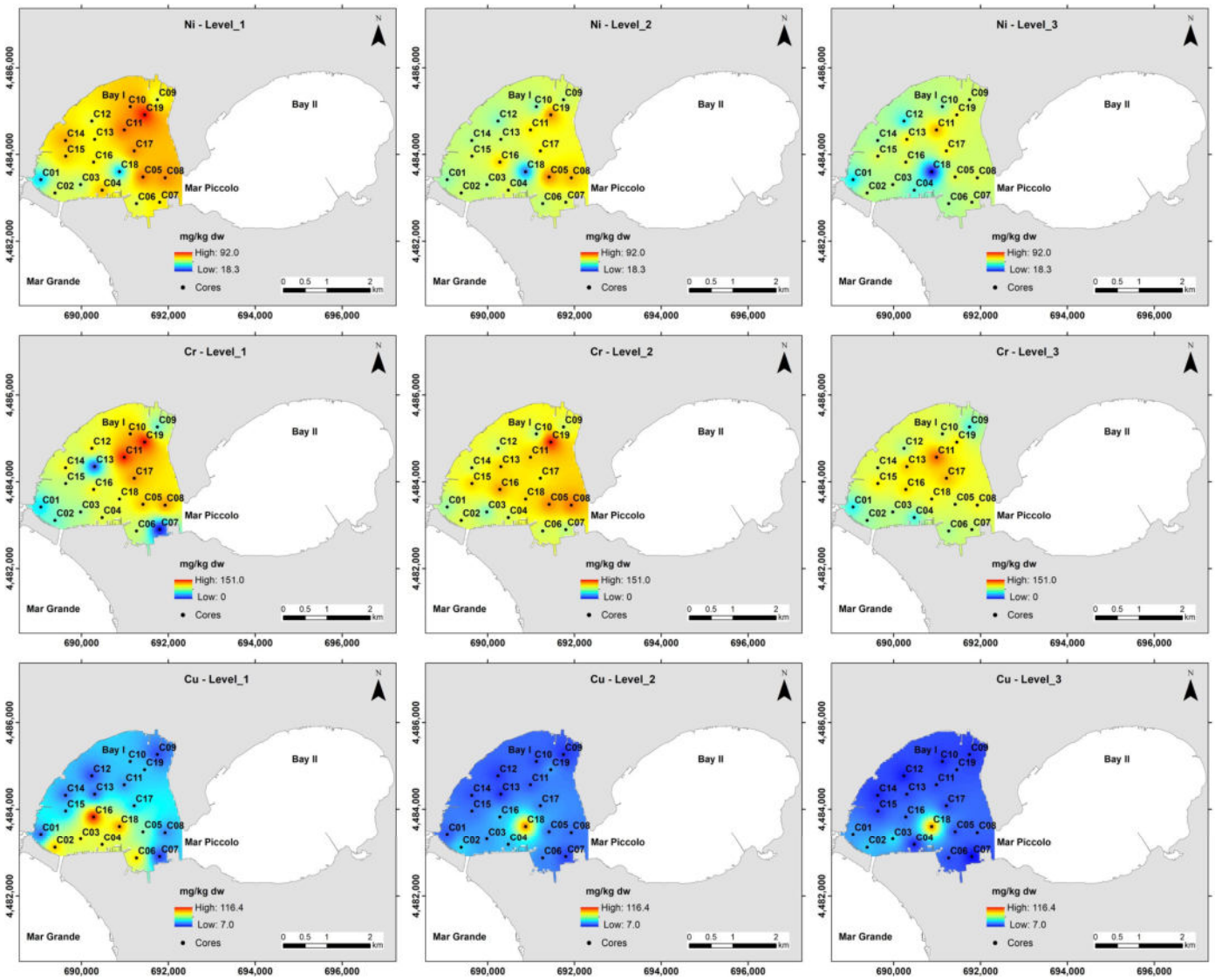

Figure 6. Spatial distribution of Ni, Cr, and Cu in the Mar Piccolo basin (Bay I): the concentration of each trace metal in the three analyzed levels (≈0–0.50 m, ≈0.50–1 m, and ≈1.5–3 m) is shown in the rows ("Level_01", "Level_2", and "Level_3", respectively).

For As, Cu, Sn, and Zn, the highest concentrations are found in the cores from "Area 170 ha", while the lowest concentrations characterize the northeast and northwest sectors of the basin. Similarly, for the concentration of Pb and also for Cu, As, Sn, and Zn, the higher national limit values are not exceeded in any core.

Table 4. Inorganic compounds concentration values. Values exceeding site-specific limits are indicated in orange while values also exceed the national limits (expressed in terms of CSC—cf. Legislative Decree 152/2006) are indicated in red (CSC for sites with commercial and residential use) and in purple (CSC for sites with industrial use). Concentrations are reported in mg/kg dw. For the site-specific limits, only values for samples with a silt content < 20% have been considered.

	Level	C01	C02	C03	C04	C05	C06	C07	C08	C09	C10	C11	C12	C13	C14	C15	C16	C17	C18	C19
Hg	0–0.5 m	0.46	4.70	8.33	4.10	3.94	15.36	0.31	0.35	<LOQ	-	0.95	0.09	0.11	0.23	2.77	3.42	2.35	2.54	1.07
	0.5–1 m	0.14	1.33	0.99	0.76	0.26	0.45	0.12	0.25	<LOQ	0.05	<LOQ	<LOQ	<LOQ	0.12	0.23	0.64	0.24	0.72	0.69
	1.5–3 m	1.22	0.84	2.51	0.05	0.12	0.39	<LOQ	0.09	<LOQ	0.10	<LOQ	<LOQ	<LOQ	<LOQ	<LOQ	0.07	0.05	0.17	<LOQ
As	0–0.5 m	*7.40*	23.42	21.91	18.51	21.64	44.75	10.13	15.74	9.54	-	15.91	11.73	6.57	14.39	17.44	23.18	15.70	15.54	11.36
	0.5–1 m	*6.19*	10.49	8.55	7.26	10.01	6.34	5.25	8.05	5.35	5.54	6.29	7.48	12.51	6.81	6.53	9.96	7.38	7.72	12.87
	1.5–3 m	*10.10*	8.00	11.31	10.77	6.63	11.31	10.53	8.92	11.38	11.55	12.53	11.70	11.81	14.25	10.18	14.60	12.25	13.00	5.56
Sn	0–0.5 m	2.58	19.60	15.25	15.63	13.08	18.55	2.54	3.02	2.31	-	4.24	2.82	2.66	3.23	6.05	88.05	6.38	9.67	4.57
	0.5–1 m	1.83	6.92	3.90	3.45	2.94	2.88	2.77	2.38	1.55	2.19	2.23	2.05	2.98	2.16	2.73	7.92	2.82	3.71	3.82
	1.5–3 m	4.66	4.14	6.03	1.08	2.19	2.50	2.15	2.36	1.95	2.03	3.52	1.65	2.91	2.03	2.68	0.47	2.75	2.89	2.16
Cd	0–0.5 m	0.21	0.57	1.16	0.63	0.69	0.90	0.28	0.26	0.13	-	0.24	0.17	0.20	0.20	0.05	0.62	0.25	0.23	0.28
	0.5–1 m	0.13	0.03	0.25	0.18	0.25	0.19	0.27	0.30	0.13	0.23	0.21	0.14	0.12	0.15	0.04	0.41	0.20	0.24	0.22
	1.5–3 m	0.23	0.26	0.38	0.15	0.19	0.16	0.13	0.15	0.13	0.13	0.13	0.10	0.15	0.12	0.03	0.19	0.12	0.13	0.19
Pb	0–0.5 m	36.38	150.38	261.63	129.03	213.58	229.29	35.96	30.10	21.67		46.60	26.78	23.37	46.75	78.78	147.91	100.34	79.10	37.92
	0.5–1 m	24.78	75.06	59.33	47.53	38.40	43.56	40.81	30.09	16.52	21.60	24.57	22.16	25.67	32.51	44.08	51.76	45.74	55.89	41.89
	1.5–3 m	53.48	38.47	99.22	12.02	29.87	28.23	26.77	13.26	18.15	22.98	36.31	14.93	26.85	19.30	33.05	16.11	33.70	35.08	22.51
Zn	0–0.5 m	49.89	293.45	311.43	276.63	218.14	402.90	79.68	102.08	58.53		121.82	72.77	71.92	90.92	125.10	337.85	133.27	67.08	107.70
	0.5–1 m	46.27	72.78	65.63	69.90	83.29	64.27	62.52	86.48	42.20	52.58	57.42	50.76	67.41	57.29	67.13	157.55	105.74	34.89	91.14
	1.5–3 m	77.22	64.40	142.00	42.18	60.71	63.10	65.86	71.18	53.50	55.45	75.17	47.15	74.71	54.95	66.10	69.41	71.50	61.24	55.61
Ni	0–0.5 m	38.31	60.83	56.13	74.27	82.50	61.70	68.75	80.01	63.63	-	83.41	64.47	67.13	77.17	73.22	68.78	79.47	37.08	92.24
	0.5–1 m	51.78	58.66	55.90	62.00	81.21	57.25	61.03	75.16	57.95	50.56	69.32	50.14	59.20	55.28	60.71	72.69	67.96	29.49	79.83
	1.5–3 m	42.12	56.88	56.04	46.17	62.70	54.50	57.66	61.49	59.03	51.20	76.33	42.85	67.61	52.75	61.03	62.22	66.70	17.33	65.20
Cr	0–0.5 m	44.96	60.45	71.06	90.63	115.00	82.85	0.31	123.00	61.00	-	150.00	100.00	15.00	99.00	81.00	100.00	124.00	95.62	151.00
	0.5–1 m	65.54	83.28	60.86	80.81	119.00	78.63	72.27	123.00	80.00	74.00	103.89	78.00	104.00	82.00	103.00	114.00	95.00	101.01	141.00
	1.5–3 m	51.94	69.80	74.73	54.93	89.00	74.59	82.16	97.00	57.00	84.00	135.74	75.00	112.00	88.00	104.00	108.00	117.00	97.77	104.00
Cu	0–0.5 m	21.97	87.92	76.61	75.17	54.82	83.75	14.83	27.05	17.16	-	28.75	17.27	20.76	23.07	35.91	117.00	37.37	95.62	36.22
	0.5–1 m	18.71	38.44	29.19	34.10	23.83	24.48	14.99	22.34	12.40	16.82	18.44	13.57	12.71	17.06	22.35	34.17	25.14	101.01	28.59
	1.5–3 m	30.01	35.60	40.36	10.54	17.73	16.47	6.95	19.80	12.28	11.12	16.60	8.85	16.23	10.70	14.00	21.73	16.00	97.77	17.51

In Level_01 (0–0.5 m), the Sn content exceeds the national limit (lower CSC) in all cores, while the concentration of As exceeds both the national limit value (lower CSC) and the site-specific limit in cores C02, C03, C05, C06, and C16. The site-specific limit is exceeded for Cu in cores C02, C03, C04, C005, C6, and C16. In five cores (C02, C03, C04, C05, C06, and C16), the concentration of Zn exceeds the national limit (lower CSC), while in four cores (C11, C15, C17, and C18), its site-specific limit is also exceeded. In Level_02 (0.5–1.0 m), the concentration of Zn exceeds the lower CSC value in core C16, while the Sn content exceeds the national limit (lower CSC) in all cores. In Level_03 (1.5–3 m) in core C03, the concentrations of As, Cu, and Sn have a peak, and the concentration of Zn exceeds the site-specific limit. Also at this level, the Sn concentration exceeds the national limit (lower CSC) in almost all cores, except core C16, where it exceeds the site-specific limit. The concentration of Cd exceeds the site-specific limit value only in Level_01 in core C03. For what concerns the concentration of Ni and Cr, no exceedance of the highest national values is observed. In addition, their vertical distribution pattern is comparable in all the cores. Compared to the other trace metals, their concentrations do not decrease with depth since increases are observed along the vertical profile in almost all the cores. The concentrations of Cr and Ni are higher than the site-specific values for sediments with a pelitic fraction <20%, but for sediments with a pelitic fraction >20% at no level, the limit of Ni and Cr concentration is exceeded.

As described, the concentrations of the analyzed trace metals in the three levels show significant variations in their spatial and vertical distribution. To make the results more readable, an overall environmental risk evaluation is expressed here as maps that summarize the exceeding of reference limit values. The maps shown in Figure 7a–c clearly display the hot-spot areas in Bay I of the Mar Piccolo basin.

The maps allow to highlight that the upper layer of marine sediments (≈0–0.5 m) in the southernmost part of the basin, mainly corresponding with the "Area 170 ha", displays very high and high-risk levels since the concentrations of several trace metals largely exceed the law limits (Table 1). The highest concentrations of As, Sn, Zn, Pb, and Hg overall lead to a very-high risk level around the cores C03 and C06 (Figure 7). The high environmental risk is mainly due to Sn, Zn, Pb, and Hg concentrations that exceed the national limits. In addition to these areas, the maps show a diffuse medium environmental risk in Bay I, mainly due to the Sn and Hg concentrations higher than the lower CSC values and to Cr and Ni concentrations that exceed the Taranto site-specific action levels everywhere. Both the Level_02 and Level_03 sediment layers present a diffusely low environmental risk, even if the medium level affects the deepest layers up to 3 m from the water-sediment interface. This condition, which characterizes mostly the southwestern sector (Figure 7b,c), is mainly due to the Sn and Hg concentrations. The presence of concentrations exceeding both site-specific and lower CSC values can be related to local phenomena of mixing of the most superficial, unconsolidated soft sediments [61], due mostly to the maritime activities carried out in the basin, whose impacts are also evident from the analysis of the morpho-bathymetric data [42,62,63]

To define the thickness and the main geometries of the Holocene sedimentary units, the sub-bottom profiles were accurately interpreted. In particular, SBP data (Figure 8) allowed to highlight the presence of a reflector parallel to the seabed, which can be interpreted as the lower limit of the most recent, coarser, non-stratified, and less consistent sediments. This uppermost stratigraphic unit includes both the 1st LTU and the uppermost of the 2nd LTU, as identified in [27]. According to the sedimentology and paleogeographic studies carried out by these authors, the uppermost sedimentary deposits have a fluid consistency and were deposited in recent times in a semi-enclosed basin with low hydrodynamism. They are considered the result of the last transgression and continuous vertical aggradation [31].

Through the interpolation of the limiting line identifying the lower limit of the uppermost stratigraphic unit interpreted by the SBP data, the digital model of the most superficial sediment layer in Bay I of the Mar Piccolo basin was obtained. This sedimentary body has a less competent thickness (of the order of 0.5–1 m) near the shoreline in the north-western

and south parts of the area, while it presents a greater thickness (ranging from 1.5 to 3 m) in almost the whole bay. In the proximity of the military shipyard in the northern part and the Punta Penne bridge in the southeastern part of Bay I, the thickness reaches values higher than 3 m and up to 7 m (Figure 9).

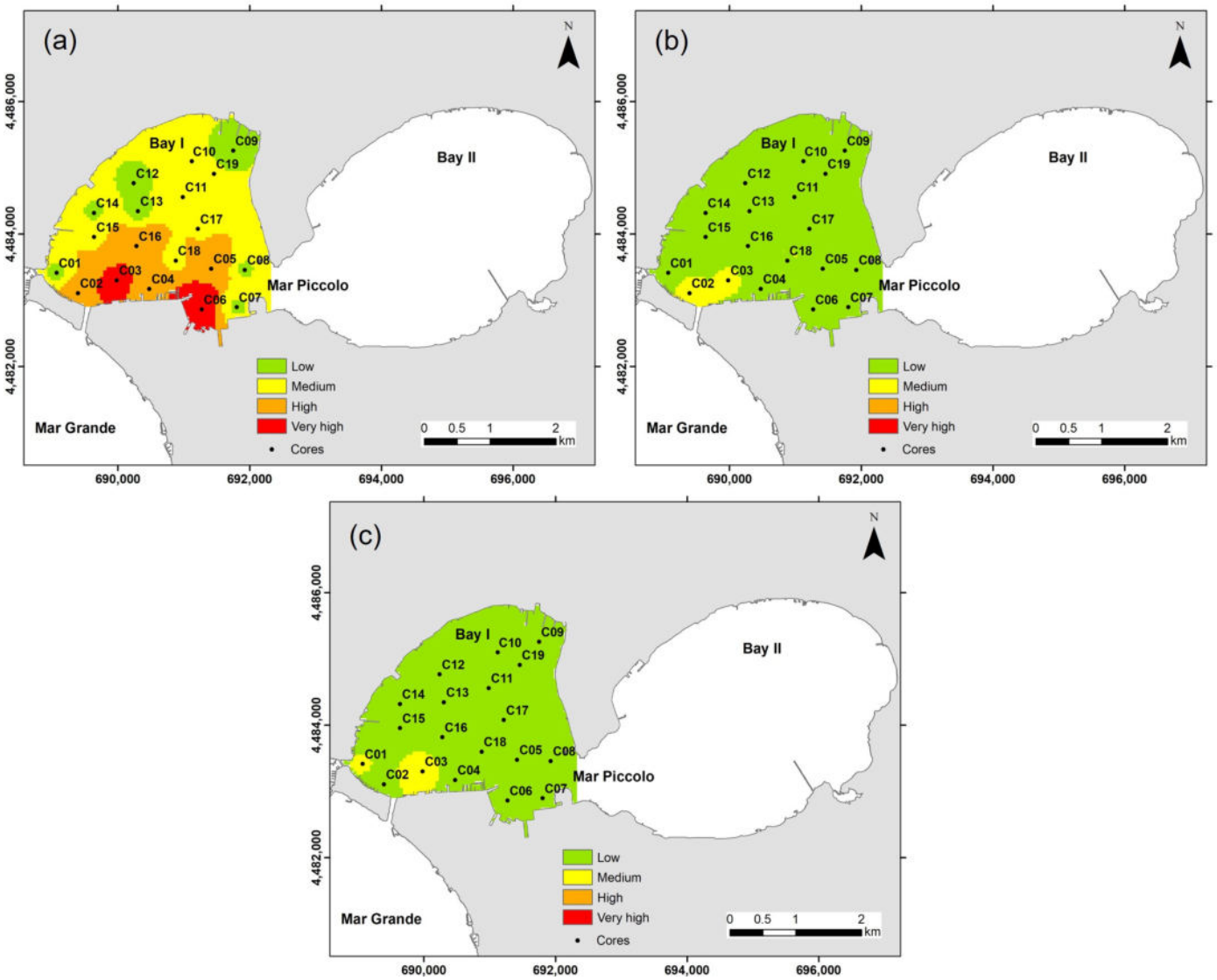

Figure 7. Map of the environmental risk level due to the exceeding of the site-specific and national limit values of the inorganic compounds in (**a**) the most superficial sediment layer (≈0–0.50 m), (**b**) the second sediment layer (≈0.50–1 m), and (**c**) the third sediment layer (≈1.50–3 m) in the Mar Piccolo basin (Bay I). In (**a**) very high values are located near the cores C03 and C06 and high values are in the southernmost part of the bay; in (**b**) and (**c**) medium risk level is located around the cores C01 and C03 in the southwestern part of Bay I.

The PCA results extracted three principal components (PC1–PC3), explaining 86% of the total variance. The PCA referring to metal concentrations in 3 sediment layers is shown in Figures 10 and 11. Factor 1 and Factor 2 explained over 76% of the total variance; in particular, factor 1 explained 59% of the total variance and was characterized by high loadings of the variables As, Zn, Cd, Pb, Hg, and Cu (0.90, 0.97, 0.90, 0.94, 0.91, and 0.74, respectively). Factor 2 explained 17% of the total variance, and Ni and Cr showed high positive loading values (0.89 and 0.79, respectively). The two-dimensional scatterplot showed on PC1 three discrete clusters (Figure 11). One cluster containing the most superficial sediment layers (0–0.50 m) from stations 6, 3, 14, 5, 4, and 2 is characterized

by high levels of As, Zn, Cd, Pb, Hg, and Cu; another cluster associated with all the other layers of the other stations is characterized by lower concentrations of the same metals. Finally, the deepest layer of sediments from station 7 is characterized by even lower levels.

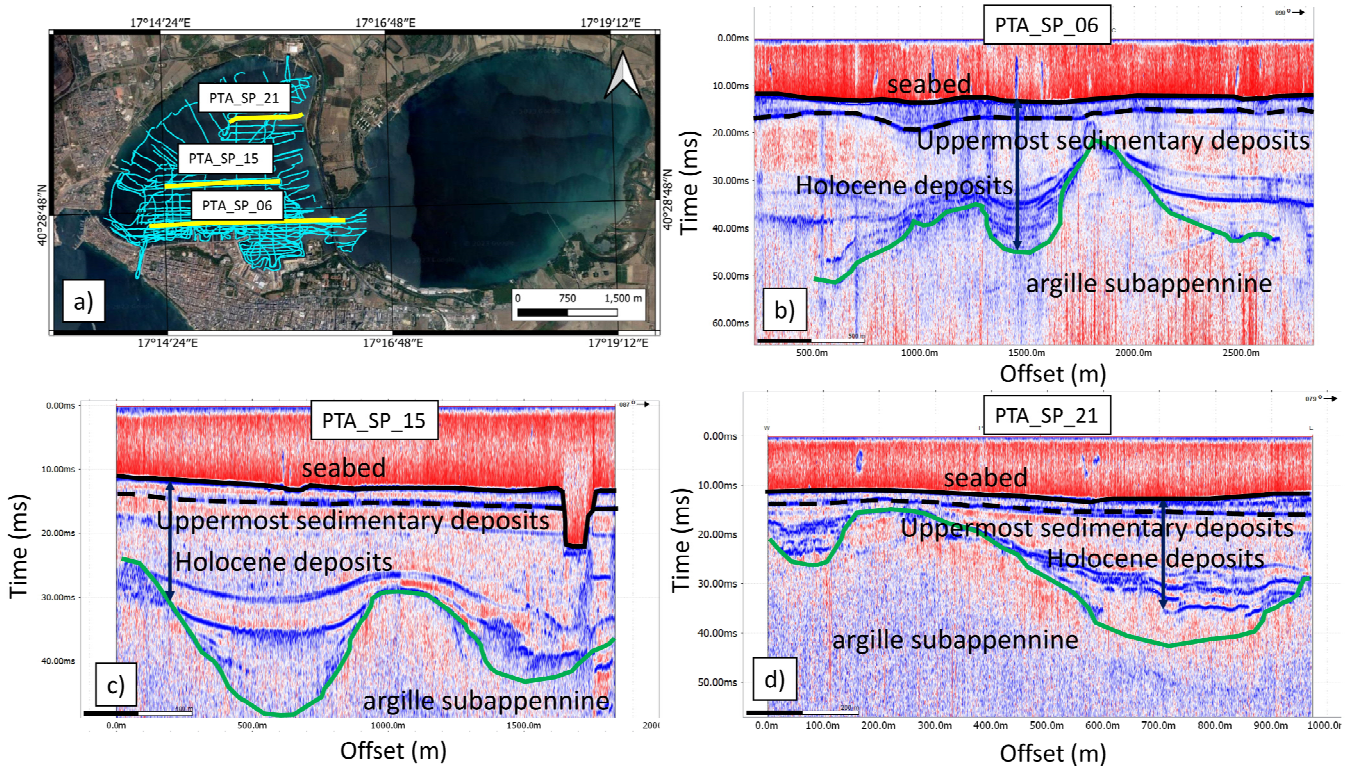

Figure 8. Sub-bottom profiles of the Mar Piccolo basin; (**a**) traces of SBP in Bay I; (**b**) SBP seismic section PTA_SP_06; (**c**) SBP seismic section PTA_SP_15; (**d**) SBP seismic section PTA_SL_21.

The significant, and positive, correlations between Cr and Ni in PC2 and the more or less uniform distribution along the different depths of sediment analyzed at all stations could suggest that they were mainly derived from natural sources.

The results obtained by applying the pollution indices allowed us to understand the degree of contamination in Bay I of Mar Piccolo Bay.

Table 5 shows that, in the first level of deep, almost all contaminants had a mean Igeo value in the unpolluted class. Only Hg has the mean Igeo value falling in the strongly polluted class (Igeo = 3.6); in fact, the extremely polluted class was individuated for Hg in the core from C02 to C06 and in the C16, while in the other cores, the Igeo value ranged from unpolluted (only in C012) to "from strongly polluted to extremely polluted" class. In the second layer, only Hg had a mean Igeo value in the moderately polluted class, with Igeo values of C02 and C03 in the strongly polluted class. All the other contaminants had a mean Igeo value falling into the unpolluted class. In the third layer, almost all contaminants were in the unpolluted class, and only Hg had an Igeo mean value in the class "from unpolluted to moderately polluted"; however, it showed an Igeo value ranging from class 0 to 4 in the C03.

The EF values (Table 5) in the first layer were always >1.5 for Hg, almost always >1.5 for Cu, and over the threshold in several cores for As, Cd, Pb, Sn, and Zn. Then the mean EF values were exceptionally high for Hg and slightly over the threshold for Cu, Sn, and Zn. The higher values are on the southern side of the bay, which indicates that anthropogenic pollution is not uniformly distributed in the study area. In the second layer, the EF value was >1.5 for Hg in almost all cores, with a mean value of 7.33. For all other contaminants, the EF values were almost always below the threshold, thus the source of the metal is due to natural weathering processes. In the third layer, the Hg had an EF mean value > 1.5 and

very high values in C01, C02, and C03. Among the other contaminants, only Cu (in C18) and Pb (in C03) showed an EF value slightly over the 1.5 threshold.

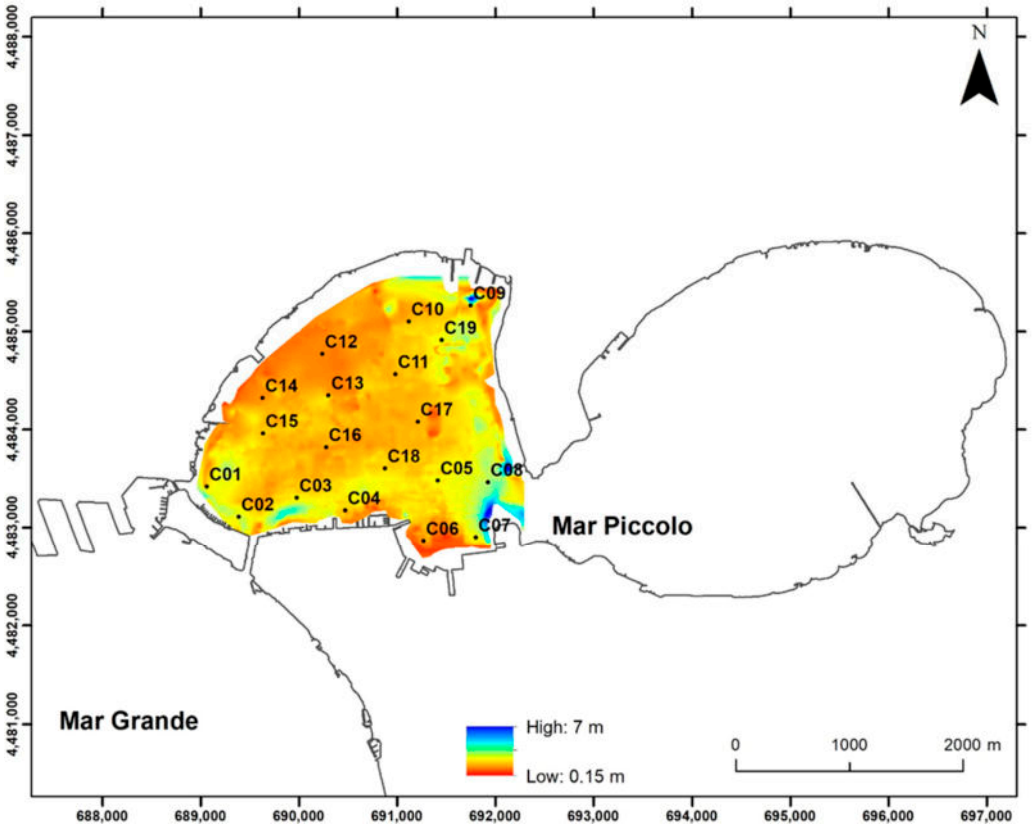

Figure 9. The digital model of the thickness of the uppermost sedimentary unit in the Mar Piccolo basin.

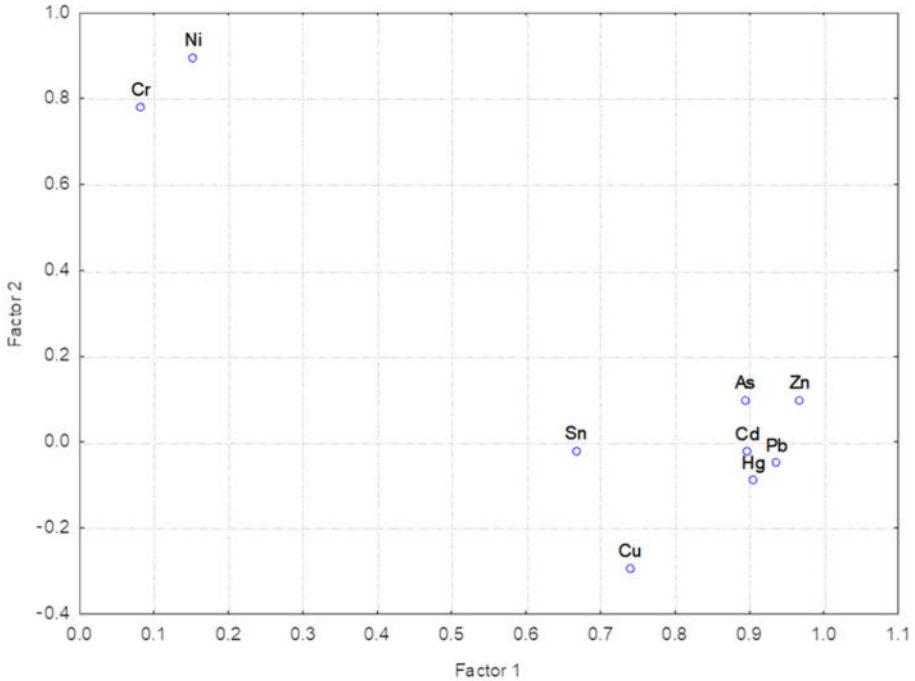

Figure 10. Loading of the variables on the first two principal components.

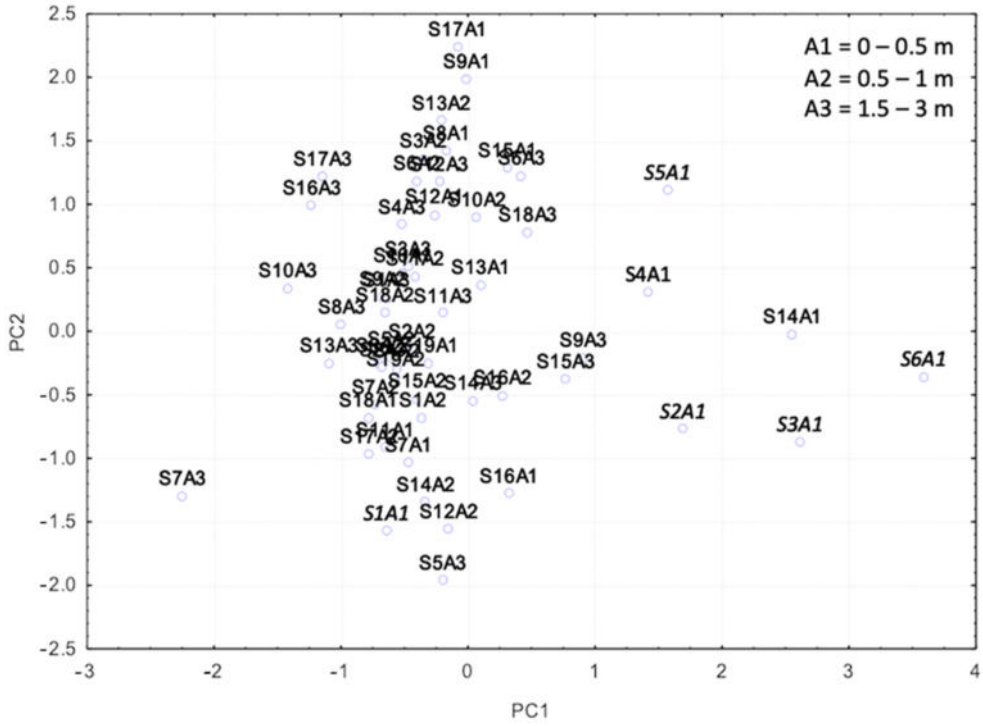

Figure 11. Scatter plot of the scores on the first two principal components obtained using As, Zn, Cd, Pb, Hg Ni, Cr, and Cu.

For what concerns the Cf, the mean values for the contaminants in the first layer appear in the following sequence: Hg > Sn > Zn > Pb > Cd > As > Ni > Cr > Cu, with only the Hg having a Cf > 6 and therefore representing a very high contamination factor and all the other pollutants in class "moderate" (Cf ranging from 1.03 to 2.04). In the second layer, the Cf mean values follow a different sequence: Hg > Cr > Ni > Zn > Pb > Cd > As > Cu > Sn, with Hg characterized by the highest mean Cf value (6.66), Cr and Ni in the class "moderate" (Cf = 1.14 and Cf = 1.07, respectively), and all the other pollutants characterized by a low contamination factor (Cf < 1). Finally, the sequence of the Cf mean values in the third level is Hg > Cr > Ni > As > Zn > Cd > Pb > Cu > Sn, with Hg having the highest value (Cf = 7.29), Cr in the "moderate" class (Cf = 1.09) and all the other pollutants in the very low class (Cf ranging from 0.44 to 0.98).

For what concerns the mCd, in the first layer, the mean value is 5.75 (0.59 < mCd < 26.8), and therefore the overall class of the superficial sediment is associated with a high degree of contamination. The highest mCd values have been calculated for the cores C03 and C06, to which a very high degree and an extremely high degree of contamination level are associated, while the minimum values have been calculated for the cores C9, C12, and C13 (mCd < 1). In the second layer, the mean mCd value is 1.26 (0.59 < mCd < 2.9), with the cores C01, C05–C15, and C17 having a mCd < 1.5 (very low degree of contamination) and cores C02, C03, and C13 higher than 2 (moderate degree of contamination). The third layer presents a mean value of 1.10 (0.51 < mCd < 4.9), with cores C04-C19 having a mCd value lower than 1.5 and cores C01 and C02 with moderate contamination. In the third layer, core C03 has the highest mCd value.

Instead, for what concerns the pollution load index (PLI), the mean estimated values are 1.74, 0.82, and 0.71 for the first, second, and third layers, respectively. Considering the values for each core, values lower than 1 have been estimated for cores C01, C07, C09, C12–C14 in the first layer, C01, C04–C15, and C17 in the second layer, and C04–C19 in the third layer. For all the remaining cores, high PLI values ranging from 1.1 to 3.43 have been estimated, suggesting that strong anthropogenic inputs characterize the sampled zones.

Table 5. Geoaccumulation index (Igeo) and enrichment factor (EF) values in the three sediment layers analyzed in this study (0–0.5 m, 0.50–1 m and 1.5–3 m).

Level	Cores	As		Cd		Cr		Cu		Hg		Ni		Pb		Sn		Zn	
		Igeo	EF	Igeo	EF	Igeo	EF	Igeo	EF	Igeo	EF	Igeo	EF	Igeo	EF	Igeo	EF	Igeo	EF
0–0.5 m	**C01**	−1.398	1.263	−1.100	1.553	−1.434	1.232	−1.682	2.123	2.131	14.583	−1.158	1.492	−1.283	1.368	−1.803	0.954	−1.544	1.141
	C02	0.264	1.669	0.341	1.760	−1.007	0.691	0.319	1.192	5.484	62.204	−0.491	0.989	0.765	2.361	1.123	3.026	1.012	2.803
	C03	0.168	1.842	1.366	4.225	−0.774	0.959	0.120	1.652	6.310	130.040	−0.607	1.076	1.564	4.846	0.761	2.777	1.098	3.509
	C04	−0.075	1.071	0.485	1.580	−0.423	0.842	0.092	1.451	5.287	44.073	−0.203	0.980	0.544	1.646	0.796	1.960	0.927	2.146
	C05	0.150	0.896	0.617	1.238	−0.079	0.764	−0.363	1.317	5.230	30.307	−0.052	0.779	1.271	1.949	0.539	1.174	0.584	1.211
	C06	1.198	3.564	1.000	3.106	−0.552	1.059	0.249	1.825	7.193	227.188	−0.471	1.121	1.373	4.024	1.043	3.201	1.469	4.300
	C07	−0.945	0.633	−0.684	0.758	−8.614	0.003	−2.249	0.005	1.562	3.597	−0.315	0.980	−1.299	0.495	−1.825	0.344	−0.869	0.667
	C08	−0.309	0.825	−0.791	0.590	0.018	1.034	−1.382	1.782	1.737	3.405	−0.096	0.956	−1.556	0.347	−1.575	0.343	−0.511	0.717
	C09	−1.031	0.608	−1.791	0.359	−0.994	0.624	−2.038	1.075	-	-	−0.426	0.924	−2.030	0.304	−1.962	0.319	−1.314	0.500
	C10	-	-	-	-	-	-	-	-	-	-	-	-	-	-	-	-	-	-
	C11	−0.294	0.732	−0.907	0.478	0.304	1.107	−1.294	1.908	3.178	8.113	−0.036	0.875	−0.925	0.472	−1.086	0.422	−0.256	0.751
	C12	−0.733	0.828	−1.404	0.520	−0.281	1.134	−2.030	1.954	−0.222	1.180	−0.407	1.038	−1.725	0.417	−1.674	0.432	−1.000	0.689
	C13	−1.570	0.574	−1.170	0.757	−3.018	0.210	−1.763	0.362	0.067	1.784	−0.349	1.337	−1.921	0.450	−1.758	0.503	−1.017	0.842
	C14	−0.438	1.327	−1.170	0.799	−0.295	1.465	−1.612	2.525	1.131	3.938	−0.148	1.623	−0.921	0.950	−1.478	0.645	−0.678	1.123
	C15	−0.161	1.913	−3.170	0.238	−0.585	1.426	−0.973	2.457	4.721	56.416	−0.224	1.831	−0.168	1.904	−0.573	1.438	−0.218	1.839
	C16	0.249	1.381	0.462	1.601	−0.281	0.956	0.731	1.648	5.026	37.840	−0.314	0.935	0.741	1.942	3.290	11.366	1.215	2.698
	C17	−0.313	1.012	−0.848	0.698	0.029	1.282	−0.916	2.210	4.484	28.121	−0.105	1.168	0.181	1.425	−0.496	0.891	−0.127	1.151
	C18	−0.327	0.905	−0.968	0.581	−0.346	0.894	0.440	1.541	4.596	27.480	−1.205	0.493	−0.162	1.015	0.104	1.221	−1.117	0.524
	C19	−0.780	0.577	−0.684	0.616	0.314	1.231	−0.961	2.122	3.349	10.095	0.109	1.069	−1.223	0.424	−0.978	0.503	−0.434	0.733
	Mean	−0.352	1.201	−0.579	1.192	−1.001	0.940	−0.851	1.619	3.604	40.610	−0.361	1.092	−0.376	1.463	−0.420	1.751	−0.154	1.519
0.5–1 m	**C01**	−1.66	0.688	−1.79	0.626	−0.89	1.169	−1.91	0.575	0.42	2.891	−0.72	1.313	−1.84	0.607	−2.30	0.441	−1.65	0.689
	C02	−0.89	1.006	−4.17	0.104	−0.54	1.282	−0.87	1.020	3.66	23.699	−0.54	1.284	−0.24	1.587	−0.38	1.439	−1.00	0.936
	C03	−1.19	0.903	−0.85	1.144	−1.00	1.032	−1.27	0.853	3.24	19.423	−0.61	1.347	−0.58	1.381	−1.21	0.893	−1.15	0.929
	C04	−1.43	0.556	−1.32	0.598	−0.59	0.994	−1.05	0.723	2.86	10.816	−0.46	1.084	−0.90	0.803	−1.38	0.573	−1.06	0.718
	C05	−0.96	0.452	−0.85	0.489	−0.03	0.862	−1.57	0.298	1.31	2.180	−0.07	0.836	−1.20	0.382	−1.61	0.288	−0.80	0.504
	C06	−1.62	0.616	−1.24	0.800	−0.63	1.227	−1.53	0.658	2.10	8.123	−0.58	1.269	−1.02	0.933	−1.64	0.607	−1.18	0.837
	C07	−1.89	0.435	−0.74	0.968	−0.75	0.960	−2.23	0.343	0.19	1.844	−0.49	1.152	−1.12	0.744	−1.70	0.497	−1.22	0.694
	C08	−1.28	0.535	−0.58	0.864	0.02	1.313	−1.66	0.411	1.25	3.087	−0.19	1.140	−1.56	0.441	−1.92	0.343	−0.75	0.771
	C09	−1.87	0.550	−1.79	0.579	−0.60	1.321	−2.51	0.353	-	-	−0.56	1.359	−2.42	0.374	−2.54	0.345	−1.79	0.582
	C10		0.576	−0.97	1.036	−0.72	1.234	−2.07	0.483	−1.07	0.965	−0.76	1.199	−2.03	0.495	−2.04	0.493	−1.47	0.732
	C11	−1.63	0.479	−1.10	0.693	−0.23	1.270	−1.93	0.388	-	-	−0.30	1.204	−1.85	0.412	−2.01	0.368	−1.34	0.586
	C12	−1.38	0.782	−1.68	0.634	−0.64	1.308	−2.38	0.392	-	-	−0.77	1.195	−2.00	0.510	−2.13	0.464	−1.52	0.711
	C13	−0.64	1.011	−1.91	0.420	−0.22	1.349	−2.47	0.284	-	-	−0.53	1.091	−1.79	0.457	−1.59	0.522	−1.11	0.730
	C14	−1.52	0.722	−1.58	0.689	−0.57	1.394	−2.05	0.500	0.19	2.361	−0.63	1.336	−1.44	0.759	−2.06	0.496	−1.34	0.814
	C15	−1.58	0.566	−3.49	0.150	−0.24	1.433	−1.66	0.536	1.13	3.702	−0.49	1.200	−1.01	0.842	−1.72	0.513	−1.12	0.780
	C16	−0.97	0.686	−0.13	1.224	−0.09	1.261	−1.04	0.651	2.61	8.191	−0.23	1.143	−0.77	0.786	−0.18	1.183	0.11	1.455
	C17	−1.40	0.650	−1.17	0.763	−0.35	1.343	−1.49	0.612	1.19	3.926	−0.33	1.365	−0.95	0.888	−1.67	0.538	−0.46	1.248
	C18	−1.34	0.725	−0.91	0.977	−0.27	1.523	0.52	2.624	2.78	12.559	−1.54	0.632	−0.66	1.157	−1.28	0.755	−2.06	0.439
	C19	−0.60	0.622	−1.03	0.461	0.21	1.094	−1.30	0.382	2.72	6.195	−0.10	0.880	−1.08	0.446	−1.24	0.400	−0.67	0.591
	Mean	−1.32	0.661	−1.44	0.696	−0.43	1.230	−1.60	0.636	1.64	7.331	−0.52	1.159	−1.29	0.737	−1.61	0.587	−1.14	0.776
1.5–3 m	**C01**	−0.95	1.18	−0.97	1.16	−1.23	0.97	−1.23	0.97	26.43	2.891	−1.02	1.12	−0.73	1.37	−0.95	1.18	−0.91	1.21
	C02	−1.29	0.77	−0.79	1.09	−0.80	1.08	−0.99	0.95	15.10	23.699	−0.59	1.26	−1.20	0.82	−1.12	0.87	−1.18	0.84
	C03	−0.79	1.00	−0.24	1.46	−0.70	1.06	−0.80	0.99	41.29	19.423	−0.61	1.13	0.16	1.94	−0.58	1.16	−0.04	1.69
	C04	−0.86	1.03	−1.58	0.62	−1.15	0.84	−2.74	0.28	0.89	10.816	−0.89	1.01	−2.88	0.25	−3.06	0.22	−1.79	0.54
	C05	−1.56	0.42	−1.24	0.52	−0.45	0.90	−1.99	0.31	1.40	2.180	−0.45	0.90	−1.57	0.41	−2.04	0.30	−1.26	0.51
	C06	−0.79	1.16	−1.49	0.71	−0.70	1.23	−2.10	0.47	7.44	8.123	−0.65	1.28	−1.65	0.64	−1.85	0.56	−1.21	0.87
	C07	−0.89	0.63	−1.79	0.34	−0.56	0.79	−3.34	0.11	0.00	1.844	−0.57	0.78	−1.73	0.35	−2.07	0.28	−1.14	0.53

Table 5. *Cont.*

Level	Cores	As		Cd		Cr		Cu		Hg		Ni		Pb		Sn		Zn	
		Igeo	EF	Igeo	EF	Igeo	EF	Igeo	EF	Igeo	EF	Igeo	EF	Igeo	EF	Igeo	EF	Igeo	EF
1.5–3 m	**C08**	−1.13	0.71	−1.58	0.52	−0.32	1.24	−1.83	0.44	1.33	3.087	−0.48	1.12	−2.74	0.23	−1.93	0.41	−1.03	0.76
	C09	−0.78	0.89	−1.79	0.44	−1.09	0.72	−2.52	0.27	-	-	−0.53	1.06	−2.29	0.31	−2.21	0.33	−1.44	0.56
	C10	-	1.09	−1.79	0.53	−0.53	1.27	−2.66	0.29	1.75	0.965	−0.74	1.10	−1.95	0.48	−2.15	0.42	−1.39	0.70
	C11	−0.64	0.69	−1.79	0.31	0.16	1.19	−2.09	0.25	-	-	−0.16	0.95	−1.29	0.44	−1.35	0.42	−0.95	0.55
	C12	−0.74	1.30	−2.17	0.48	−0.70	1.34	−2.99	0.27	-	-	−1.00	1.09	−2.57	0.37	−2.45	0.40	−1.63	0.70
	C13	−0.72	0.85	−1.58	0.47	−0.12	1.29	−2.12	0.32	-	-	−0.34	1.11	−1.72	0.43	−1.63	0.45	−0.96	0.72
	C14	−0.45	1.42	−1.91	0.52	−0.47	1.41	−2.72	0.29	-	2.361	−0.70	1.20	−2.20	0.42	−2.15	0.44	−1.40	0.73
	C15	−0.94	0.77	−3.91	0.10	−0.22	1.26	−2.33	0.29	-	3.702	−0.49	1.05	−1.42	0.55	−1.75	0.44	−1.14	0.67
	C16	−0.42	1.05	−1.24	0.59	−0.17	1.24	−1.70	0.43	0.93	8.191	−0.46	1.02	−2.46	0.25	−4.26	0.07	−1.07	0.67
	C17	−0.67	0.81	−1.91	0.34	−0.05	1.24	−2.14	0.29	0.61	3.926	−0.36	1.00	−1.39	0.49	−1.71	0.39	−1.03	0.63
	C18	−0.58	0.89	−1.79	0.39	−0.31	1.08	0.47	1.86	2.17	12.559	−2.30	0.27	−1.34	0.53	−1.64	0.43	−1.25	0.57
	C19	−1.81	0.40	−1.24	0.59	−0.22	1.19	−2.01	0.34	-	6.195	−0.39	1.06	−1.98	0.35	−2.06	0.33	−1.39	0.53
	Mean	−0.89	0.90	−1.62	0.59	−0.51	1.12	−1.99	0.50	8.28	7.331	−0.67	1.03	−1.73	0.56	−1.94	0.48	−1.17	0.74

Finally, Table 6 shows the ecological risk factor (Er) and ecological risk index (RI) values obtained in the three analyzed sediment layers of the 19 sampled stations. The Er is an index that evaluates, as reported earlier, the potential risk associated with a single element. As regards As, Cr, Cu, Ni, Pb, Zn, and Cd, all sampled sites in the study present a low potential ecological risk with the exception of the 0–0.50 m layer at station 3 located south of the basin in area 170 ha, which has a considerable potential ecological risk for Cd. In contrast, at all stations except stations 12, 13, and 14, there is a potential ecological risk for Hg in the 0 to 0.50 m layer ranging from high to very high. In the 0.50–1 m layer, the potential ecological risk for Hg remains at stations 2, 3, 4, 6, 16, 18, and 19, from high to very high. Finally, in the 1.5–3 m layer, the high to very high risk remains at only stations 1, 2, 3, and 6. Furthermore, the cumulative ecological risks of the studied metal, i.e., the potential ecological risk index (RI), indicated a significantly high ecological risk for most stations located in the south and center of the basin to a depth of up to one meter. Finally, the core C03 presents a significantly high ecological risk up to a depth of 3 m.

Table 6. Ecological risk factor (Er) and ecological risk index (RI) in the three sediment layers analyzed in this study (0–0.5 m, 0.50–1 m and 1.5–3 m).

Level	*Cores*	*Ecological Risk (Er)*								*Risk Index (RI)*
		As	**Cd**	**Cr**	**Cu**	**Hg**	**Ni**	**Pb**	**Zn**	
0–0.5 m	**C01**	6	21	1	2	263	3	3	0.5	300
	C02	18	57	1	9	2686	5	13	3.0	2793
	C03	17	116	2	8	4760	5	22	3.2	4933
	C04	14	63	2	8	2343	7	11	2.9	2451
	C05	17	69	3	6	2251	7	18	2.2	2373
	C06	34	90	2	9	8777	5	19	4.2	8942
	C07	8	28	0	2	177	6	3	0.8	224
	C08	12	26	3	3	200	7	3	1.1	255
	C09	7	13	2	2	-	6	2	0.6	32
	C10	-	-	-	-	-	-	-	-	-
	C11	12	24	4	3	543	7	4	1.3	598
	C12	9	17	2	2	51	6	2	0.8	90
	C13	5	20	0	2	63	6	2	0.7	99
	C14	11	20	2	2	131	7	4	0.9	179

Table 6. *Cont.*

Level	*Cores*	*Ecological Risk (Er)*								*Risk Index (RI)*
		As	**Cd**	**Cr**	**Cu**	**Hg**	**Ni**	**Pb**	**Zn**	
0–0.5 m	**C15**	13	5	2	4	1583	6	7	1.3	1621
	C16	18	62	2	12	1954	6	13	3.5	2071
	C17	12	25	3	4	1343	7	9	1.4	1404
	C18	12	23	2	10	1451	3	7	0.7	1510
	C19	9	28	4	4	611	8	3	1.1	668
0.5–1 m	**C01**	5	13	2	2	80	5	2	0.5	108
	C02	8	3	2	4	760	5	6	0.8	789
	C03	7	25	2	3	566	5	5	0.7	613
	C04	6	18	2	4	434	5	4	0.7	474
	C05	8	25	3	3	149	7	3	0.9	198
	C06	5	19	2	3	257	5	4	0.7	295
	C07	4	27	2	2	69	5	3	0.6	112
	C08	6	30	3	2	143	7	3	0.9	194
	C09	4	13	2	1	ND	5	1	0.4	27
	C10	4	23	2	2	29	4	2	0.5	66
	C11	5	21	3	2	ND	6	2	0.6	39
	C12	6	14	2	1	ND	4	2	0.5	30
	C13	10	12	3	1	ND	5	2	0.7	34
	C14	5	15	2	2	69	5	3	0.6	101
	C15	5	4	3	2	131	5	4	0.7	155
	C16	8	41	3	4	366	6	4	1.6	433
	C17	6	20	2	3	137	6	4	1.1	179
	C18	6	24	2	11	411	3	5	0.4	462
	C19	10	22	3	3	394	7	4	0.9	0.9
1.5–3 m	**C01**	8	23	1	3	697	4	5	0.8	741
	C02	6	26	2	4	480	5	3	0.7	527
	C03	9	38	2	4	1434	5	8	1.5	1502
	C04	8	15	1	1	29	4	1	0.4	60
	C05	5	19	2	2	69	5	3	0.6	105
	C06	9	16	2	2	223	5	2	0.7	259
	C07	8	13	2	1	ND	5	2	0.7	32
	C08	7	15	2	2	51	5	1	0.7	85
	C09	9	13	1	1	0	5	2	0.6	32
	C10	9	13	2	1	57	4	2	0.6	89
	C11	10	13	3	2	ND	7	3	0.8	38
	C12	9	10	2	1	ND	4	1	0.5	27
	C13	9	15	3	2	ND	6	2	0.8	38
	C14	11	12	2	1	ND	5	2	0.6	33
	C15	8	3	3	1	ND	5	3	0.7	24
	C16	11	19	3	2	40	5	1	0.7	83
	C17	9	12	3	2	29	6	3	0.7	64
	C18	10	13	2	10	97	2	3	0.6	138
	C19	4	19	3	2	ND	6	2	0.6	36

5. Discussion

The results of the analyses carried out in this study highlight that Bay I of the Mar Piccolo basin is affected by a strong contamination level due to both the high concentrations of some trace metals, which in some cases are above the national limits, and to their concurrence. The evidence of this latter is clearly illustrated in the risk maps shown in Figure 7, where the hot-spot areas, corresponding to the high and very high-risk zones at Level_01, are shown in orange and red, respectively, and the medium-risk area at Level_02 and Level_03 are shown in in yellow. These areas are mainly situated in the central and southernmost part of the Bay I and are located next to the industrial sites and the shipyards and dockyards pertaining to the Italian Navy. Thus, trace metal contamination is not limited to the first 50 cm of sediments; it affects all of the soft uppermost Holocene sediments. In fact, by taking into account the sediment thickness evaluated from the analysis of the SBP data, it is clear that the soft uppermost Holocene sediments, whose thickness ranges from a few centimeters to 3 m, are highly affected by resuspension and reworking processes. Given their fluid consistency, these sediments have most likely been reworked and/or resuspended: the analysis of the sea floor digital terrain model, coupled with the morphological interpretation of the SSS data [63], shows the presence of grooves, probably due to the crossing of larger ships and the dragging of ship anchors that cause strong circulation flow and the soft mud sediment movement, mostly in the southernmost part of Bay I.

As a consequence, they can represent a further source of pollution for the sea floor and marine fauna [27]. Such processes are strongly enhanced by anthropogenic maritime activities carried out in the basin, such as mussel farming, anchoring, fishing, and marine infrastructure. Therefore, the crossing of larger ships that affected Bay I related to the presence of naval bases and shipyards can induce a significant impact on the soft uppermost marine sediment layer, mainly in the "Area 170 ha". Thus, the anthropogenic impacts on coastal areas may not be limited to the direct release of contaminants from urban and industrial districts but may also influence the natural sedimentation process.

Unfortunately, the anthropogenic impact on this area is bound to last for a long time since the natural hydrodynamism that characterizes the Mar Piccolo basin is related to limited input and output flows through the two narrow channels and to the freshwater springs that flow in the northern sector of Bay I [64]. It is easy to connect the extreme and high environmental risk levels with the concentration of Hg, Sn, As, Pb, Cd, Zn, and Cu due to anthropogenic maritime activities near the southern coast, as confirmed by the PCA analysis results. According to these results, Ni and Cr could be of natural origin, and their higher concentration in the central part of Bay I is probably due to both the water circulation in the bottom layer of Bay I [33] and the sentiment thickness ranging between 1.5 and 3 m. The water circulation allows contaminants to spread throughout the basin; therefore, based on the time needed for the water masses exchange, which considers the new water coming in from both the sea and the rivers discharging and the single particle flowing into the basin until it leaves it [34], the central part of Bay I has a higher sensitivity to water masses stagnation and is especially vulnerable to pollution. Moreover, the low sediment thickness can produce an increase in these trace metal concentrations with respect to other parts of the bay. The current hydrodynamic conditions and the consequent effect of currents in terms of bottom stress may be modified by climate change. Currently, the basin shows a low-energy hydrodynamic regime and, consequently, a low tendency to bottom erosion [33,34]. Nevertheless, ongoing research activities are focusing on the evaluation of the expected bottom stress values under climate change conditions in order to identify areas where sediment and pollutant re-suspension can be more relevant. This last aspect is particularly relevant from an ecological perspective since fate, bioavailability, and bioaccumulation processes are expected to be modified by climate drivers. The assessment of the interactions between climate change and contaminants must be considered in an integrated manner to define the vulnerability of coastal and marine ecosystems and preserve their functions and services [65].

For what concerns the comparison of the content of the trace metals for which the concentration is above the national limits (Hg, As, Pb, Zn) with the international guidelines, it emerges that the concentration of Hg in the first level (Level_01) is above the ERL in almost all the cores (except for Cores C11-C12-C13) and above the ERM values in all the cores, excluding cores C01, C07, C08, C12, C13, and C14. Similarly, in the second level (Level_02), the ERL values are exceeded in all the cores, except for C01, C07, C10, and C14). In the third level, ERM values are exceeded in C01, C02, C03, C06, and C18. Differently from other Italian coastal sites, where the high concentration of Hg in the sediment is attributed to the direct discharge into the aqueous media from a chlor-alkali plant, an acetaldehyde plant, and mining activities [66–68], the high content of Hg in all the analyzed layers may be attributed to the shipyard impacts in both bays of the Mar Piccolo. In addition, since mercury fulminate was widely used during the 20th century in munitions manufacturing [69], the presence of Hg in sediments in the Mar Piccolo, where military facilities are present, may not be unusual.

The concentration of As in the first and third layers exceeds the international guide value (ERL) in all the cores except for C01, C09, and C13, and C05 and C19, respectively, in the first and third layers. In the second layer, it is exceeded in cores C02, C03, C05, C13, C16, and C19.

Similarly, the concentration of Pb is above the ERL values in C02, C03, C04, C05, C06, C14, C15, C16, C17, and C18 in the first level, in C02, C03, C04, C16, and C19 in the second layer, and in C03 in the third layer. The ERM value is not exceeded. Finally, the concentration of Zn exceeds the ERL value in six cores in the first level (C02-C06, and C16) and in one core in the second layer (C16). Moreover, in this case, the ERM value is not exceeded.

In addition, the potential ecological risk index associated with the metals found that the area of Bay I of the Mar Piccolo from the south to the center has a very high ecological risk, which may influence the contamination risk for residing flora and fauna and trophic transfer to human consumption. Indeed, several authors [70] report a human health risk associated with the consumption of seafood caught in Bay I of the Mar Piccolo.

The results shown in this study can be considered very useful to assess the spatial distribution of trace metals and identify the most vulnerable zones in Bay I of the Mar Piccolo basin. Nevertheless, more investigations are required to evaluate the potential correlation between the pollutant concentrations and specific sediment characteristics (i.e., granulometric composition, organic content) in order to provide new insights in the distribution of trace metals as a consequence of chemical–physical conditions, as carried out for a few sediment cores analyzed by Petronio et al. [71]. In particular, the definition of the granulometric composition as well as organic content is also important in treatment engineering and in the definition of the most suitable remediation strategies, as highlighted in Rudovica et al. [72]. In this context, the interpretation of SBP data is very useful to identify and map the main seismic horizons that, together with the first reflector representing the seabed, constitute the upper limits of specific sismo-facies characterized by specific sediment content. The direct sediment sample characterization, coupled with the seismic profiles' interpretation, allows for defining the 3D model of well-defined sedimentary facies.

Previous characterization of the Taranto coastal area by the national and regional authorities focused on the evaluation of the contamination of the first sediment layers and pointed out that high concentrations of one or more inorganic contaminants, exceeding the site-specific threshold values, were present in a large part of Bay I. The results of such characterization have been synthesized in [27], where the distribution of the contaminants assessed by ISPRA (Institute for Environmental Protection and Research) in 2010 has been mapped. According to that analysis, Hg is the most widespread contaminant, with concentration values that exceed even the national limit in the central part of Bay I. A high concentration of trace elements (e.g., Pb, Cu, and Zn) was also estimated. Nevertheless, previous activities did not provide the complete spatial distribution of the trace metal concentration in the whole of Bay I. In fact, as highlighted in [27], the characterization activities were performed

in the northern and central parts of Bay I. In addition, the concentrations were evaluated in terms of exceeding site-specific and national limits for each contaminant, but no data on the co-occurrence of exceeding limits were provided. The results of this study can therefore be considered an important step toward complete knowledge of the contamination of both surficial and sub-surficial sediments in the whole of Bay I of the Mar Piccolo basin, laying the foundations for planning tailored remediation activities.

Compared with other coastal areas of the Italian SINs [3,19,73–75], the peculiar characteristics of the Mar Piccolo basin make the environmental situation of Bay I more complex and its natural recovery very far from being achieved. Comparable features could be found in the lagoonal SIN, such as the SIN "Venezia-Porto Marghera", which is a semi-enclosed coastal basin located in northeastern Italy; nevertheless, in this case, deeper canals isolate the different zones and act as a boundary inhibiting the transport of pollutants [5]. In other coastal Italian SINs, physical parameters such as wave motion, sea currents, and deeper water may promote favorable hydrodynamic processes that support the self-purification and recovery processes. This is the case of the Italian SIN "Falconara Marittima", where the most recent analyses have suggested a natural recovery of the marine area over two decades of restrictions on human activities [75].

Several international case studies have analyzed the environmental conditions of marine sediments both in lagoonal areas [11,12] and in semi-enclosed marine basins [76]. In all these cases, the wave motion, the sea currents, and the ocean tides play a fundamental role in self-purification and marine recovery processes.

6. Conclusions

In this study, new insights on the distribution of trace metals in Bay I of the Mar Piccolo basin are provided by analyzing chemical and geophysical data acquired with the aim of selecting the most adequate remediation activities. In detail, superficial and sub-surficial marine sediments from 19 cores have been analyzed. Samples were representative of three sediment layers (Level_01 from the seabed to 0.5 m; Level_2 from 0.5 to 1 m; and Level_3 from 1.5 to 3 m). Furthermore, in order to define the thickness of the most recent sediment unit, sub-bottom profile data have been interpreted. The results allowed us to identify the most compromised cores in terms of trace metal contamination and explain their distribution. Thus, the cores located south-east of the old city of Taranto and those located in the "Area 170 ha present levels of Hg, Cd, As, Sn, Pb, Cu, Cr, Ni, and Zn higher than the site-specific limits. In addition, cores C06 and C03, located in the "Area 170 ha", result in being the only cores with Hg concentrations exceeding the highest CSC limit values, and then there is an ecological risk in the Mar Piccolo basin, especially related to Hg.

The results of our study highlight the relevant role played by the multidisciplinary analysis of the high-resolution geophysical data coupled with the sedimentological interpretation of the core samples in the characterization of the submerged sedimentary architectures. This study is also preparatory to the description of potential environmental risk scenarios related to the resuspension and spread of contaminants, whose modeling is currently under investigation. The easily readable maps proposed can sensitize local authorities and communities with respect to potential threats derived from marine sediment pollution, and these results represent the scientific basis for identifying the most appropriate remediation strategies necessary to define management actions aimed at promoting the recovery and sustainable use of the analyzed coastal area.

Author Contributions: Data curation, F.D.G., G.S. (Giovanni Scardino), A.D.L., A.M. and A.R.; formal analysis, A.D.L., F.D.G., G.S. (Giovanni Scardino), A.R. and A.M.; methodology, A.R., A.M. and G.S. (Giovanni Scicchitano); writing—original draft, A.M., A.R., A.D.L. and G.S. (Giovanni Scardino); writing—review and editing, A.D.L., G.S. (Giovanni Scardino), G.S. (Giovanni Scicchitano), D.C., M.M., G.M., S.L., A.M. and A.R.; supervision, G.S. (Giovanni Scicchitano) and A.D.L.; project administration, A.R. All authors have read and agreed to the published version of the manuscript.

Funding: This research was funded by the Apulia Region (Italy) under the European Regional Development Fund and the European Social Fund (POR Puglia FESR-FSE 2014-2020)-Action 10.4 "Research for Innovation" (REFIN). Research project reference number: FC44BB89. Scientific responsible: Angela Rizzo. Furthermore, this study was carried out within the RETURN Extended Partnership and received funding from the European Union Next-GenerationEU (National Recovery and Resilience Plan—NRRP, Mission 4, Component 2, Investment 1.3—D.D. 1243 2/8/2022, PE0000005).

Data Availability Statement: The data presented in this study are available on request from the corresponding author.

Acknowledgments: The authors are grateful to the Special Commissioner for urgent measurements of reclamation, environmental improvements, and redevelopment of Taranto, Vera Corbelli, who coordinated the characterization activities carried out in the Taranto area during the period 2015-2017 in the frame of the Collaboration Agreement "Activities of common interest preparatory to the implementation of the interventions for the reclamation, environmentalisation, and requalification of the Mar Piccolo of Taranto". The authors would like to thank Angelo Tursi and Vito Felice Uricchio, as Scientific Managers of the above-mentioned Collaboration Agreement. In detail, data used in this study are derived from the surveys performed during activities envisaged in "Phase G" and "Phase H" of the Collaboration Agreement (Scientific responsible of "Phase G" activities: Giuseppe Mastronuzzi; Scientific responsible of "Phase H" activities: Nicola Cardellicchio and Giuseppe Mascolo).

Conflicts of Interest: The authors declare no conflict of interest.

References

1. Zhao, Y.; Xu, M.; Liu, Q.; Wang, Z.; Zhao, L.; Chen, Y. Study of Heavy Metal Pollution, Ecological Risk and Source Apportionment in the Surface Water and Sediments of the Jiangsu Coastal Region, China: A Case Study of the Sheyang Estuary. *Mar. Pollut. Bull.* **2018**, *137*, 601–609. [CrossRef]
2. Zhang, Z.; Lu, Y.; Li, H.; Tu, Y.; Liu, B.; Yang, Z. Assessment of Heavy Metal Contamination, Distribution and Source Identification in the Sediments from the Zijiang River, China. *Sci. Total Environ.* **2018**, *645*, 235–243. [CrossRef]
3. Ausili, A.; Bergamin, L.; Romano, E. Environmental Status of Italian Coastal Marine Areas Affected by Long History of Contamination. *Front. Environ. Sci.* **2020**, *8*. [CrossRef]
4. Tnoumi, A.; Angelone, M.; Armiento, G.; Caprioli, R.; Crovato, C.; De Cassan, M.; Montereali, M.R.; Nardi, E.; Parrella, L.; Proposito, M.; et al. Heavy Metal Content and Potential Ecological Risk Assessment of Sediments from Khnifiss Lagoon National Park (Morocco). *Environ. Monit. Assess.* **2022**, *194*, 356. [CrossRef] [PubMed]
5. Zonta, R.; Botter, M.; Cassin, D.; Pini, R.; Scattolin, M.; Zaggia, L. Sediment Chemical Contamination of a Shallow Water Area Close to the Industrial Zone of Porto Marghera (Venice Lagoon, Italy). *Mar. Pollut. Bull.* **2007**, *55*, 529–542. [CrossRef] [PubMed]
6. Liu, M.; Zhang, A.; Liao, Y.; Chen, B.; Fan, D. The Environment Quality of Heavy Metals in Sediments from the Central Bohai Sea. *Mar. Pollut. Bull.* **2015**, *100*, 534–543. [CrossRef] [PubMed]
7. Liu, S.; Shi, X.; Yang, G.; Khokiattiwong, S.; Kornkanitnan, N. Concentration Distribution and Assessment of Heavy Metals in the Surface Sediments of the Western Gulf of Thailand. *Environ. Earth Sci.* **2016**, *75*, 346. [CrossRef]
8. Trifuoggi, M.; Donadio, C.; Mangoni, O.; Ferrara, L.; Bolinesi, F.; Nastro, R.A.; Stanislao, C.; Toscanesi, M.; Di Natale, G.; Arienzo, M. Distribution and Enrichment of Trace Metals in Surface Marine Sediments in the Gulf of Pozzuoli and off the Coast of the Brownfield Metallurgical Site of Ilva of Bagnoli (Campania, Italy). *Mar. Pollut. Bull.* **2017**, *124*, 502–511. [CrossRef] [PubMed]
9. Pandey, L.K.; Park, J.; Son, D.H.; Kim, W.; Islam, M.S.; Choi, S.; Lee, H.; Han, T. Assessment of Metal Contamination in Water and Sediments from Major Rivers in South Korea from 2008 to 2015. *Sci. Total Environ.* **2019**, *651*, 323–333. [CrossRef] [PubMed]
10. Fathollahzadeh, H.; Kaczala, F.; Bhatnagar, A.; Hogland, W. Significance of Environmental Dredging on Metal Mobility from Contaminated Sediments in the Oskarshamn Harbor, Sweden. *Chemosphere* **2014**, *119C*, 445–451. [CrossRef] [PubMed]
11. Beraldi, G.Q.F.; de Rezende, C.E.; de Almeida, M.G.; Carvalho, C.; de Lacerda, L.D.; de Farias, R.N.; Vidal, M.; Souza, M.D.P.; Molisani, M.M. Assessment of a Coastal Lagoon Metal Distribution through Natural and Anthropogenic Processes (SE, Brazil). *Mar. Pollut. Bull.* **2019**, *146*, 552–561. [CrossRef] [PubMed]
12. Xian, H.; Dong, X.; Wang, Y.; Li, Y.; Xing, J.; Jeppesen, E. Geochemical Baseline Establishment and Pollution Assessment of Heavy Metals in the Largest Coastal Lagoon (Pinqing Lagoon) in China Mainland. *Mar. Pollut. Bull.* **2022**, *177*, 113459. [CrossRef] [PubMed]
13. Ausili, A.; Romano, E.; Mumelter, E.; Tornato, A. Stato Dell'arte Sulle Bonifiche Delle Aree Marine e Di Transizione Interne Ai SIN. In Proceedings of the Workshop "Siti Contaminati. Esperienze Negli Interventi di Risanamento", Taormina, Italy, 9–11 February 2012; pp. 27–45.
14. Bonsignore, M.; Tamburrino, S.; Oliveri, E.; Marchetti, A.; Durante, C.; Berni, A.; Quinci, E.; Sprovieri, M. Tracing Mercury Pathways in Augusta Bay (Southern Italy) by Total Concentration and Isotope Determination. *Environ. Pollut.* **2015**, *205*, 178–185. [CrossRef] [PubMed]

15. Di Leonardo, R.; Mazzola, A.; Tramati, C.D.; Vaccaro, A.; Vizzini, S. Highly Contaminated Areas as Sources of Pollution for Adjoining Ecosystems: The Case of Augusta Bay (Central Mediterranean). *Mar. Pollut. Bull.* **2014**, *89*, 417–426. [CrossRef] [PubMed]
16. Di Leonardo, R.; Adelfio, G.; Bellanca, A.; Chiodi, M.; Mazzola, S. Analysis and Assessment of Trace Element Contamination in Offshore Sediments of the Augusta Bay (SE Sicily): A Multivariate Statistical Approach Based on Canonical Correlation Analysis and Mixture Density Estimation Approach. *J. Sea Res.* **2014**, *85*, 428–442. [CrossRef]
17. Romano, E.; Bergamin, L.; Ausili, A.; Celia Magno, M.; Gabellini, M. Evolution of the Anthropogenic Impact in the Augusta Harbor (Eastern Sicily, Italy) in the Last Decades: Benthic Foraminifera as Indicators of Environmental Status. *Environ. Sci. Pollut. Res.* **2016**, *23*, 10514–10528. [CrossRef] [PubMed]
18. Romano, E.; Bergamin, L.; Croudace, I.W.; Pierfranceschi, G.; Sesta, G.; Ausili, A. Measuring Anthropogenic Impacts on an Industrialised Coastal Marine Area Using Chemical and Textural Signatures in Sediments: A Case Study of Augusta Harbour (Sicily, Italy). *Sci. Total Environ.* **2021**, *755*, 142683. [CrossRef]
19. Arienzo, M.; Donadio, C.; Mangoni, O.; Bolinesi, F.; Stanislao, C.; Trifuoggi, M.; Toscanesi, M.; Di Natale, G.; Ferrara, L. Characterization and Source Apportionment of Polycyclic Aromatic Hydrocarbons (Pahs) in the Sediments of Gulf of Pozzuoli (Campania, Italy). *Mar. Pollut. Bull.* **2017**, *124*, 480–487. [CrossRef]
20. Romano, E.; Ausili, A.; Zharova, N.; Celia Magno, M.; Pavoni, B.; Gabellini, M. Marine Sediment Contamination of an Industrial Site at Port of Bagnoli, Gulf of Naples, Southern Italy. *Mar. Pollut. Bull.* **2004**, *49*, 487–495. [CrossRef]
21. Romano, E.; Bergamin, L.; Ausili, A.; Pierfranceschi, G.; Maggi, C.; Sesta, G.; Gabellini, M. The Impact of the Bagnoli Industrial Site (Naples, Italy) on Sea-Bottom Environment. Chemical and Textural Features of Sediments and the Related Response of Benthic Foraminifera. *Mar. Pollut. Bull.* **2009**, *59*, 245–256. [CrossRef]
22. Romano, E.; Bergamin, L.; Celia Magno, M.; Pierfranceschi, G.; Ausili, A. Temporal Changes of Metal and Trace Element Contamination in Marine Sediments Due to a Steel Plant: The Case Study of Bagnoli (Naples, Italy). *Appl. Geochem.* **2018**, *88*, 85–94. [CrossRef]
23. Sprovieri, M.; Passaro, S.; Ausili, A.; Bergamin, L.; Finoia, M.G.; Gherardi, S.; Molisso, F.; Quinci, E.M.; Sacchi, M.; Sesta, G.; et al. Integrated Approach of Multiple Environmental Datasets for the Assessment of Sediment Contamination in Marine Areas Affected by Long-Lasting Industrial Activity: The Case Study of Bagnoli (Southern Italy). *J. Soils Sediments* **2020**, *20*, 1692–1705. [CrossRef]
24. Buccolieri, A.; Buccolieri, G.; Cardellicchio, N.; Dell'Atti, A.; Di Leo, A.; Maci, A. Heavy Metals in Marine Sediments of Taranto Gulf (Ionian Sea, Southern Italy). *Mar. Chem.* **2006**, *99*, 227–235. [CrossRef]
25. Vitone, C.; Federico, A.; Puzrin, A.M.; Ploetze, M.; Carrassi, E.; Todaro, F. On the Geotechnical Characterisation of the Polluted Submarine Sediments from Taranto. *Environ. Sci. Pollut. Res.* **2016**, *23*, 12535–12553. [CrossRef] [PubMed]
26. Vitone, C.; Sollecito, F.; Todaro, F.; Corbelli, V. Contaminated Marine Sites: Geotechnical Issues Bridging the Gap between Characterisation and Remedial Strategies. *Riv. Ital. Geotec.* **2020**, *2020*, 41–62. [CrossRef]
27. Cotecchia, F.; Vitone, C.; Sollecito, F.; Mali, M.; Miccoli, D.; Petti, R.; Milella, D.; Ruggieri, G.; Bottiglieri, O.; Santaloia, F.; et al. A Geo-Chemo-Mechanical Study of a Highly Polluted Marine System (Taranto, Italy) for the Enhancement of the Conceptual Site Model. *Sci. Rep.* **2021**, *11*, 4017. [CrossRef] [PubMed]
28. Ciaranfi, N.; Pieri, P.; Ricchetti, G. Note Alla Carta Geologica Delle Murge e Del Salento (Puglia Centromeridionale). *Mem. Della Soc. Geol. Ital.* **1988**, *41*, 449–460.
29. Negri, A.; Amorosi, A.; Antonioli, F.; Bertini, A.; Florindo, F.; Lurcock, P.C.; Marabini, S.; Mastronuzzi, G.; Regattieri, E.; Rossi, V.; et al. A Potential Global Boundary Stratotype Section and Point (GSSP) for the Tarentian Stage, Upper Pleistocene, from the Taranto Area (Italy): Results and Future Perspectives. *Quat. Int.* **2015**, *383*, 145–157. [CrossRef]
30. Lisco, S.; Corselli, C.; De Giosa, F.; Mastronuzzi, G.; Moretti, M.; Siniscalchi, A.; Marchese, F.; Bracchi, V.; Tessarolo, C.; Tursi, A. Geology of Mar Piccolo, Taranto (Southern Italy): The Physical Basis for Remediation of a Polluted Marine Area. *J. Maps* **2016**, *12*, 173–180. [CrossRef]
31. Valenzano, E.; Scardino, G.; Cipriano, G.; Fago, P.; Capolongo, D.; De Giosa, F.; Lisco, S.; Mele, D.; Moretti, M.; Mastronuzzi, G. Holocene Morpho-Sedimentary Evolution of the Mar Piccolo Basin (Taranto, Southern Italy). *Geogr. Fis. E Din. Quat.* **2018**, *41*, 119–135. [CrossRef]
32. Dominik, J.; Leoni, S.; Cassin, D.; Guarneri, I.; Bellucci, L.G.; Zonta, R. Eutrophication History and Organic Carbon Burial Rate Recorded in Sediment Cores from the Mar Piccolo of Taranto (Italy). *Environ. Sci. Pollut. Res.* **2023**, *30*, 56713–56730. [CrossRef] [PubMed]
33. Pascalis, F.D.; Petrizzo, A.; Ghezzo, M.; Lorenzetti, G.; Manfè, G.; Alabiso, G.; Zaggia, L. Estuarine Circulation in the Taranto Seas. *Environ. Sci. Pollut. Res.* **2016**, *23*, 12515–12534. [CrossRef] [PubMed]
34. De Serio, F.; Armenio, E.; Ben Meftah, M.; Capasso, G.; Corbelli, V.; De Padova, D.; De Pascalis, F.; Di Bernardino, A.; Leuzzi, G.; Monti, P.; et al. Detecting Sensitive Areas in Confined Shallow Basins. *Environ. Model. Softw.* **2020**, *126*, 104659. [CrossRef]
35. Caroppo, C.; Giordano, L.; Palmieri, N.; Bellio, G.; Portacci, G.; Hopkins, T.S.; Sclafani, P.; Bisci, A.P. Progress Toward Sustainable Mussel Aquaculture in Mar Piccolo, Italy. *Ecol. Soc.* **2012**, *17*, 10. [CrossRef]
36. Bracchi, V.; Marchese, F.; Savini, A.; Chimienti, G.; Mastrototaro, F.; Tessarolo, C.; Cardone, F.; Tursi, A.; Corselli, C. Seafloor Integrity of the Mar Piccolo Basin (Southern Italy): Quantifying Anthropogenic Impact. *J. Maps* **2016**, *12*, 1–11. [CrossRef]

37. Tursi, A.; Corbelli, V.; Cipriano, G.; Capasso, G.; Velardo, R.; Chimienti, G. Mega-Litter and Remediation: The Case of Mar Piccolo of Taranto (Ionian Sea). *Rend. Fis. Acc. Lincei* **2018**, *29*, 817–824. [CrossRef]
38. ISPRA. *Evaluation of Characterization Results for the Identification of Appropriate Actions for Remediation of Site of National Interest of Taranto*; Technical Report; ISPRA: Roma, Italy, 2010; p. 90.
39. Parenzan, P. Il Mar Piccolo e Il Mar Grande Di Taranto. Carta Biocenotica. *Thalass. Salentina* **1969**, *3*, 19–34.
40. Mastrototaro, F.; D'Onghia, G. Spatial and Seasonal Distribution of Ascidians in a Semi-Enclosed Basin of the Mediterranean Sea. *J. Mar. Biol. Assoc.* **2008**, *88*, 1053–1061. [CrossRef]
41. Pierri, C.; Lazic, T.; Corriero, G.; Cardone, F.; Onen Tarantini, S.; Desiderato, A.; Mirto, S.; Gristina, M. Site Fidelity of Hippocampus Guttulatus Cuvier, 1829 at Mar Piccolo of Taranto (Southern Italy; Ionian Sea). *Environ. Biol Fish* **2020**, *103*, 1105–1118. [CrossRef]
42. Rizzo, A.; De Giosa, F.; Di Leo, A.; Lisco, S.; Moretti, M.; Scardino, G.; Scicchitano, G.; Mastronuzzi, G. Geo-Environmental Characterisation of High Contaminated Coastal Sites: The Analysis of Past Experiences in Taranto (Southern Italy) as a Key for Defining Operational Guidelines. *Land* **2022**, *11*, 878. [CrossRef]
43. Muller, G. Index of Geoaccumulation in Sediments of the Rhine River. *GeoJournal* **1969**, *2*, 108–118.
44. Muller, G. The Heavy Metal Pollution of the Sediments of Neckars and Its Tributary: A Stocktaking. *Chem. Ztg.* **1981**, *105*, 157–164.
45. Ravichandran, M.; Baskaran, M.; Santschi, P.H.; Bianchi, T.S. History of Trace Metal Pollution in Sabine-Neches Estuary, Beaumont, Texas. *Environ. Sci. Technol.* **1995**, *29*, 1495–1503. [CrossRef]
46. Windom, H.L.; Smith, R.G.; Rawlinson, C. Particulate Trace Metal Composition and Flux across the Southeastern U.S. Continental Shelf. *Mar. Chem.* **1989**, *27*, 283–297. [CrossRef]
47. Din, Z.B. Use of Aluminium to Normalize Heavy-Metal Data from Estuarine and Coastal Sediments of Straits of Melaka. *Mar. Pollut. Bull.* **1992**, *24*, 484–491. [CrossRef]
48. Zhang, J.; Liu, C.L. Riverine Composition and Estuarine Geochemistry of Particulate Metals in China—Weathering Features, Anthropogenic Impact and Chemical Fluxes. *Estuar. Coast. Shelf Sci.* **2002**, *54*, 1051–1070. [CrossRef]
49. Jiang, M.; Zeng, G.; Zhang, C.; Ma, X.; Chen, M.; Zhang, J.; Lu, L.; Yu, Q.; Hu, L.; Liu, L. Assessment of Heavy Metal Contamination in the Surrounding Soils and Surface Sediments in Xiawangang River, Qingshuitang District. *PLoS ONE* **2013**, *8*, e71176. [CrossRef] [PubMed]
50. Kerolli-Mustafa, M.; Ćurković, L. Analysing the Characteristics and Application Potentials of Jarosite Waste in Kosovo. *Glob. Nest J.* **2016**, *18*, 89–97.
51. Hakanson, L. An Ecological Risk Index for Aquatic Pollution Control.a Sedimentological Approach. *Water Res.* **1980**, *14*, 975–1001. [CrossRef]
52. Abrahim, G.M.S.; Parker, R.J. Assessment of Heavy Metal Enrichment Factors and the Degree of Contamination in Marine Sediments from Tamaki Estuary, Auckland, New Zealand. *Environ. Monit. Assess.* **2008**, *136*, 227–238. [CrossRef]
53. Tomlinson, D.L.; Wilson, J.G.; Harris, C.R.; Jeffrey, D.W. Problems in the Assessment of Heavy-Metal Levels in Estuaries and the Formation of a Pollution Index. *Helgol. Meeresunters* **1980**, *33*, 566–575. [CrossRef]
54. Badr, N.B.E.; El-Fiky, A.A.; Mostafa, A.R.; Al-Mur, B.A. Metal Pollution Records in Core Sediments of Some Red Sea Coastal Areas, Kingdom of Saudi Arabia. *Environ. Monit. Assess.* **2009**, *155*, 509–526. [CrossRef] [PubMed]
55. Sekabira, K.; Origa, H.O.; Basamba, T.A.; Mutumba, G.; Kakudidi, E. Assessment of Heavy Metal Pollution in the Urban Stream Sediments and Its Tributaries. *Int. J. Environ. Sci. Technol.* **2010**, *7*, 435–446. [CrossRef]
56. Niu, Y.; Jiang, X.; Wang, K.; Xia, J.; Jiao, W.; Niu, Y.; Yu, H. Meta Analysis of Heavy Metal Pollution and Sources in Surface Sediments of Lake Taihu, China. *Sci. Total Environ.* **2020**, *700*, 134509. [CrossRef] [PubMed]
57. Liu, Y.; Zhang, K.; Xu, S.; Yan, M.; Tao, D.; Chen, L.; Wei, Y.; Wu, C.; Liu, G.; Lam, P.K.S. Heavy Metals in the "Plastisphere" of Marine Microplastics: Adsorption Mechanisms and Composite Risk. *Gondwana Res.* **2022**, *108*, 171–180. [CrossRef]
58. Turekian, K.K.; Wedepohl, K.H. Distribution of the Elements in Some Major Units of the Earth's Crust. *GSA Bull.* **1961**, *72*, 175–192. [CrossRef]
59. Long, E.R.; Macdonald, D.D.; Smith, S.L.; Calder, F.D. Incidence of Adverse Biological Effects within Ranges of Chemical Concentrations in Marine and Estuarine Sediments. *Environ. Manag.* **1995**, *19*, 81–97. [CrossRef]
60. Macdonald, D.D.; Carr, R.S.; Calder, F.D.; Long, E.R.; Ingersoll, C.G. Development and Evaluation of Sediment Quality Guidelines for Florida Coastal Waters. *Ecotoxicology* **1996**, *5*, 253–278. [CrossRef]
61. Massari, F.; Cotugno, P.; Tursi, A.; Milella, P.; Lisco, S.; Scardino, G.; Scicchitano, G.; Rizzo, A.; Valenzano, E.; Moretti, M.; et al. Mapping of Organotin Compounds in Sediments of Mar Piccolo (Taranto, Italy) Using Gas Chromatography-Mass Spectrometry Analysis and Geochemical Data. In Proceedings of the 2021 International Workshop on Metrology for the Sea; Learning to Measure Sea Health Parameters (MetroSea), Reggio Calabria, Italy, 4–6 October 2021; pp. 21–26.
62. Scardino, G.; De Giosa, F.; D'Onghia, M.; Demonte, P.; Fago, P.; Saccotelli, G.; Valenzano, E.; Moretti, M.; Velardo, R.; Capasso, G.; et al. The Footprints of the Wreckage of the Italian Royal Navy Battleship Leonardo Da Vinci on the Mar Piccolo Sea-Bottom (Taranto, Southern Italy). *Oceans* **2020**, *1*, 77–93. [CrossRef]
63. Rizzo, A.; De Giosa, F.; Donadio, C.; Scardino, G.; Scicchitano, G.; Terracciano, S.; Mastronuzzi, G. Morpho-Bathymetric Acoustic Surveys as a Tool for Mapping Traces of Anthropogenic Activities on the Seafloor: The Case Study of the Taranto Area, Southern Italy. *Mar. Pollut. Bull.* **2022**, *185*, 114314. [CrossRef]

64. Mossa, M.; Armenio, E.; Meftah, M.B.; Bruno, M.F.; De Padova, D.; De Serio, F. Meteorological and Hydrodynamic Data in the Mar Grande and Mar Piccolo, Italy, of the Coastal Engineering Laboratory (LIC) Survey, Winter and Summer 2015. *Earth Syst. Sci. Data* **2021**, *13*, 599–607. [CrossRef]
65. Hatje, V.; Sarin, M.; Sander, S.G.; Omanović, D.; Ramachandran, P.; Völker, C.; Barra, R.O.; Tagliabue, A. Emergent Interactive Effects of Climate Change and Contaminants in Coastal and Ocean Ecosystems. *Front. Mar. Sci.* **2022**, *9*. [CrossRef]
66. Covelli, S.; Emili, A.; Acquavita, A.; Koron, N.; Faganeli, J. Benthic Biogeochemical Cycling of Mercury in Two Contaminated Northern Adriatic Coastal Lagoons. *Cont. Shelf Res.* **2011**, *31*, 1777–1789. [CrossRef]
67. Covelli, S.; Petranich, E.; Pavoni, E.; Signore, S. Can Sediments Contaminated by Mining Be a Source of Mercury in the Coastal Environment Due to Dredging? Evidence from Thermo-Desorption and Chemical Speciation. *Bull. Environ. Contam. Toxicol.* **2021**, *106*, 942–948. [CrossRef] [PubMed]
68. Emili, A.; Acquavita, A.; Covelli, S.; Spada, L.; Di Leo, A.; Giandomenico, S.; Cardellicchio, N. Mobility of Heavy Metals from Polluted Sediments of a Semi-Enclosed Basin: In Situ Benthic Chamber Experiments in Taranto's Mar Piccolo (Ionian Sea, Southern Italy). *Environ. Sci. Pollut. Res. Int.* **2016**, *23*, 12582–12595. [CrossRef] [PubMed]
69. Arbestain, M.C.; Rodríguez-Lado, L.; Bao, M.; Macías, F. Assessment of Mercury-Polluted Soils Adjacent to an Old Mercury-Fulminate Production Plant. *Appl. Environ. Soil. Sci.* **2008**, *2009*, e387419. [CrossRef]
70. Spada, L.; Annicchiarico, C.; Cardellicchio, N.; Giandomenico, S.; Di Leo, A. Mercury and Methylmercury Concentrations in Mediterranean Seafood and Surface Sediments, Intake Evaluation and Risk for Consumers. *Int. J. Hyg. Environ. Health* **2012**, *215*, 418–426. [CrossRef]
71. Petronio, B.M.; Cardellicchio, N.; Calace, N.; Pietroletti, M.; Pietrantonio, M.; Caliandro, L. Spatial and Temporal Heavy Metal Concentration (Cu, Pb, Zn, Hg, Fe, Mn, Hg) in Sediments of the Mar Piccolo in Taranto (Ionian Sea, Italy). *Water Air Soil. Pollut.* **2012**, *223*, 863–875. [CrossRef]
72. Rudovica, V.; Rotter, A.; Gaudêncio, S.P.; Novoveská, L.; Akgül, F.; Akslen-Hoel, L.K.; Alexandrino, D.A.M.; Anne, O.; Arbidans, L.; Atanassova, M.; et al. Valorization of Marine Waste: Use of Industrial By-Products and Beach Wrack Towards the Production of High Added-Value Products. *Front. Mar. Sci.* **2021**, *8*, 723333. [CrossRef]
73. Arienzo, M.; Toscanesi, M.; Trifuoggi, M.; Ferrara, L.; Stanislao, C.; Donadio, C.; Grazia, V.; Gionata, D.V.; Carella, F. Contaminants Bioaccumulation and Pathological Assessment in Mytilus Galloprovincialis in Coastal Waters Facing the Brownfield Site of Bagnoli, Italy. *Mar. Pollut. Bull.* **2019**, *140*, 341–352. [CrossRef]
74. ISPRA. *Rapporto Rifiuti Speciali*, 2021 ed.; Dati Di Sintesi; ISPRA: Roma, Italy, 2021; Volume 345, p. 53.
75. Corinaldesi, C.; Bianchelli, S.; Rastelli, E.; Varrella, S.; Canensi, S.; Gambi, C.; Lo Martire, M.; Musco, L.; Bertocci, I.; Fanelli, E.; et al. The Paradox of an Unpolluted Coastal Site Facing a Chronically Contaminated Industrial Area. *Front. Mar. Sci.* **2022**, *8*. [CrossRef]
76. Wu, J.; Rong, S.; Wang, M.; Lu, R.; Liu, J. Environmental Quality and Ecological Risk Assessment of Heavy Metals in the Zhuhai Coast, China. *Front. Mar. Sci.* **2022**, *9*. [CrossRef]